Science with the Athena X-ray Integral Field Unit

X-IFU Instrument Preliminary Requirement Review

Prepared By

Didier Barret
and the X-IFU Science Advisory Team

Massimo Cappi (INAF OAS), Etienne Pointecouteau (IRAP), Graziella Branduardi-Raymont (MSSL-UCL), Esra Bulbul (CFA), Mauro Dadina (INAF OAS), Anne Decourchelle (CEA-SAP), Stefano Ettori (INAF OAS), Alexis Finoguenov (Univ. Helsinki), Yasushi Fukazawa (Univ. Hiroshima), Andrea Goldwurm (APC), Agnieszka Janiuk (CTP Warsaw), Jelle Kaastra (SRON), Pasquale Mazzotta (Univ. Tor Vergata), Jon Miller (Univ. Michigan), Giovanni Miniutti (CAB (CSIC-INTA)), Yaël Nazé (Univ. Liège), Fabrizio Nicastro (INAF Obs. Roma), Gabriel W. Pratt (CEA-SAP), Joop Schaye (Leiden Obs.), Salvatore Sciortino (INAF Obs. Palermo), Aurora Simionescu (SRON), Jose Miguel Torrejon (Univ. de Alicante), Jacco Vink (Univ. Amsterdam), Joern Wilms (ECAP & Remeis Observatory)

Wednesday 9th January, 2019

XIFU-SN-XI-09012019-IRAP

1 Abstract

The X-ray Integral Field Unit (X-IFU) on board the Advanced Telescope for High-ENergy Astrophysics (Athena) will provide spatially resolved high-resolution X-ray spectroscopy from 0.2 to 12 keV, with $\sim$ 5" pixels over a field of view of 5 arc minute equivalent diameter and a spectral resolution of 2.5 eV up to 7 keV. In this paper, we first review the core scientific objectives of Athena, driving the main performance parameters of the X-IFU, namely the spectral resolution, the field of view, the effective area, the count rate capabilities, the instrumental background. We then illustrate the breakthrough potential of the X-IFU for some observatory science goals. This paper is an updated and completed version of the SPIE 2016 paper (Barret et al. 2016). A non exhaustive list of recent developments are emphasized in grey boxes. This document is intended to support the X-IFU Instrument Preliminary Requirement Review.

2 Introduction

ESA's Athena X-ray observatory mission was selected in June 2014 to address the Hot and Energetic Universe science theme (Nandra et al. 2013). The Hot Universe refers to the baryons at temperatures above 10^{5-6}K and that amount to about half of the total baryonic content of the Universe. Baryons at $T > 10^7$ K trapped in dark-matter potential wells tracing the large-scale structures of the Universe are as numerous as those locked into stars. Gas at lower temperatures (down to $T \sim 10^5$ K) is expected to reside in filamentary structures pervading the intergalactic medium. The hot gas distributed on large-scales is strongly influenced by phenomena occurring in the immediate vicinity of black holes (the Energetic Universe) through a poorly understood process called Cosmic Feedback. As X-rays are copiously produced by hot gas and accretion around black holes, the best observational handle on the Hot and Energetic Universe is through X-ray observations. In addition X-rays can escape relatively unimpeded from significantly obscured environments and are only weakly contaminated by phenomena other than those mentioned.

To address these and other science objectives Athena is conceived as a large observatory offering an unprecedented combination of sensitive X-ray imaging, timing and high-resolution spectroscopy.

The X-IFU is a cryogenic imaging spectrometer, offering spatially-resolved high-spectral resolution X-ray spectroscopy over a 5 arc minute equivalent diameter field of view (see Table 1 for the performance requirements). The breadth of the science affordable with the X-IFU encompasses key scientific issues of the Hot and Energetic Universe science theme and beyond. In a nutshell, the X-IFU will provide:

- 3D integral field spectroscopic mapping of hot cosmic plasmas, enabling measurements of gas bulk motions and turbulence, chemical abundances and the spatial distribution of these and other physical parameters. *This drives the X-IFU field of view and spatial resolution, particle background, spectral resolution and calibration accuracy.*
- Weak spectroscopic line detection, enabling the detection of unresolved absorption and emission lines from Warm and Hot Intergalactic Medium filaments and weak spectral features produced by unusual ion species or states. *This drives the X-IFU spectral resolution, low energy response, calibration and throughput.*
- Physical characterization of the Hot and Energetic Universe, including plasma diagnostics using emission line multiplets, AGN reverberation and black hole spin measurements, winds in galactic sources in outburst, AGN winds and outflows, stellar outflows, solar wind charge exchange, etc. *This drives the X-IFU spectral resolution, the high energy response, and high-count rate capability.*

In this paper we will first review the core scientific objectives of Athena as driving the X-IFU performance requirements: this will cover the Hot Universe

Table 1 – X-IFU key performance requirements.

Energy range	0.2–12.0 keV
Spectral resolution	$\leq$ 2.5 eV (up to 7.0 keV)
Non X-ray background	5×10^{-3} counts/s/cm^2/keV (2-10 keV)
2.5 eV throughput (broadband, point source)	80% at 1 mCrab (10 mCrab as a goal)
10 eV throughput (5-8 keV, point source)	50% at 1 Crab
2.5 eV throughput (broadband, extended source)	80% at 2×10^{-11} ergs/s/cm^2/arcmin^2 (0.2-12 keV)
Continuous cool time	32 hours

(section 3), the Energetic Universe (section 4), as well as the Observatory science (section 5).

3 The Hot Universe

The X-IFU on board Athena will be vital to characterise the Hot Universe, by measuring the mechanical energy stored in gas bulk motions and turbulence in groups and clusters of galaxies, the distribution of its metal abundances across cosmic time, the effect of Active Galactic Nuclei (AGN) in the intra-cluster medium (ICM) and by obtaining the distribution and properties of the warm/hot baryonic filaments in the intergalactic medium.

3.1 Cluster bulk motions and turbulence

The hierarchical growth of large-scale structures happens through continuous accretion of material and successive merging events (Bertschinger 1998; Planelles et al. 2015; Vogelsberger et al. 2014). These processes heat the gas filling the massive halos by adiabatic compression and by countless shocks they generate at all scales, e.g. Markevitch & Vikhlinin (2007).

Part of the gravitational energy released at the formation of a halo is channeled through bulk motions and turbulent flows. It cascades down to smaller scales where it is dissipated, thereby contributing to the virialisation of their hot gaseous atmosphere (McCarthy et al. 2007; Nagai et al. 2013; Lau et al. 2013). Turbulence in the ICM is also related to the weak magnetic field bathing the cluster gas and further links to the viscosity, convection and conduction of the gas (Schekochihin & Cowley 2007). The connection between these micro-scale physical processes, as well as their impact on the larger scales is still to be unveiled in order to fully understand the overarching process of assembling large scale structures.

To date this has been investigated mostly by establishing a connection between the statistics of surface brightness fluctuations and of the turbulent velocity field, e.g. Churazov et al. (2012); Zhuravleva et al. (2014); Khatri & Gaspari (2016). Direct measurement of the turbulent velocity and bulk motions can be obtained from the respective measurement of the broadening and shift they induce on the atomic emission lines from the ICM. X-ray grating spectroscopy has only provided upper limits because of the limitations of dispersive spectroscopy when pointing at extended sources, see e.g. (Sanders & Fabian 2013; Pinto et al. 2015). Thanks to the capabilities of the SXS calorimeter spectrometer *Hitomi* has provided an unprecedented view of the Perseus cluster (Mitsuda et al. 2014; Takahashi et al. 2014; Hitomi Collaboration et al. 2016), showing for the first time what spatially-resolved high-resolution X-ray spectroscopy can deliver. These unique observations

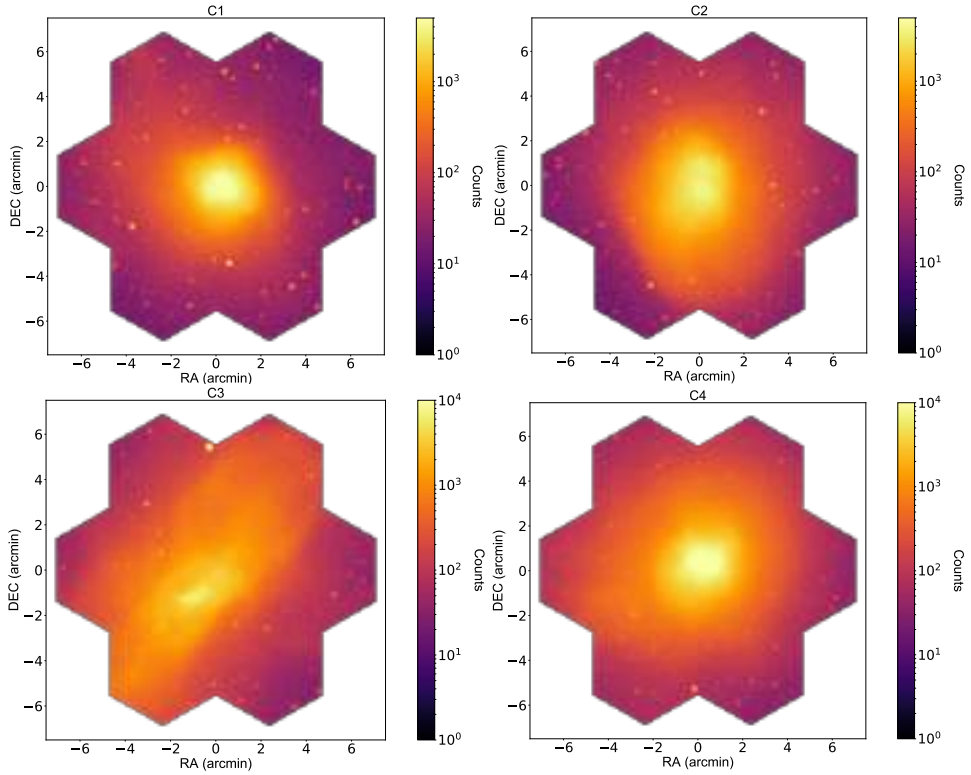

Figure 1 – Maps in number of counts per X-IFU pixel (assumed to be of 249 μm pitch) of a sample of four clusters (C1 to C4 from top left to bottom right) at redshift z = 0.1. Each mosaic is made of seven X-IFU pointings of 100ks, each simulated using the instrument end-to-end simulator SIXTE. The image is taken from Cucchetti et al. (2018). Input clusters are taken from large-scale hydrodynamical simulations performed using the GADGET-3 smoothed-particle hydrodynamics code, see Rasia et al. (2015); Biffi et al. (2018).

have shown that the level of turbulence close to the core of Perseus is rather modest ($< 164 \pm 10\,\mathrm{km\,s^{-1}}$), despite the highly structured spatial distribution of hot gas resulting from AGN feedback. This is only a small glimpse of what X-IFU will be able to do, but on 12 times smaller spatial scales and with a significantly better spectroscopic throughput (see Fig. 16, 17).

The direct measurement of the bulk motions and turbulence velocity field thus requires spatially-resolved, high resolution spectroscopy. The X-IFU on board the Athena observatory will map the velocity field of the hot gas in groups and clusters of galaxies down to a precision of $10 - 20\,\mathrm{km\,s^{-1}}$ for velocities ranging between $100 - 1000\,\mathrm{km\,s^{-1}}$ (see Fig. 1 and 2).

The joint high spatial and spectral resolution of the X-IFU shall also allow to resolve line complexes (e.g., Iron around 6.7 keV) and measure line ratios to

further constrain thermodynamics or ionisation state of the gas far out into the clusters outskirts, e.g. Molendi et al. (2016). All these diagnostics will provide us with a comprehensive view of how the dark and baryonic matter assemble and evolve into large scale potential wells.

Roncarelli et al. (2018) have assessed the capability of the X-IFU to probe the intra-cluster medium kinematics through the measurements of the gas velocity and velocity dispersion via centroid-shift and broadening of emission lines, starting from hydrodynamical simulations, including the injection of turbulence. They have shown that the five physical quantities, namely the emission measure, temperature, metal abundance, velocity, and velocity dispersion recovered matched the input projected values without bias; the systematic errors were below 5%, except for velocity dispersion whose error reaches about 15%. This was the first demonstration of the capability of the X-IFU to probe the physics of the turbulent motions of the ICM with high precision.

3.2 Chemical enrichment

With masses up to and exceeding $10^{15}\,M_{\odot}$, the deep potential wells of galaxy clusters retain all the information regarding the chemical enrichment of their intracluster medium (ICM) across cosmic time (this is not the case for galaxies, which lose their gaseous haloes and eject metals into the inter-galactic medium through stellar winds and stellar explosions). Just about 40 years ago a feature corresponding to Fe XXV and Fe XXVI transitions was discovered in the X-ray spectrum of the Perseus cluster (Mitchell et al. 1976). Since then, it has been recognised that the hot gas of the ICM is continuously enriched with heavy elements generated in type Ia (SN1a) and core-collapse supernova (SNcc) explosions in the cluster member galaxies. Elements from O to Si and S are mainly produced in massive stars and ejected in SNcc at the end of their lifetime. White dwarfs in binary systems give rise to SNIa explosions that produce elements up to Si, Fe and Ni. X-ray observations of emission lines from highly-ionized elements are the only way to access information on the abundances of the hot gas, its evolution to high redshift, and the processes by which heavy elements are redistributed into the surrounding ICM.

The combination of Athena's large effective area and the 2.5 eV spectral resolution of the X-IFU will allow the abundances of many common heavy elements to be measured to unprecedented precision. Abundance ratios are a powerful method for constraining the contribution of SN1a, SNcc and AGB stars to the total heavy element abundance, as each source produces different heavy element yields. Information on the Initial Mass Function (IMF), the stellar populations, and the

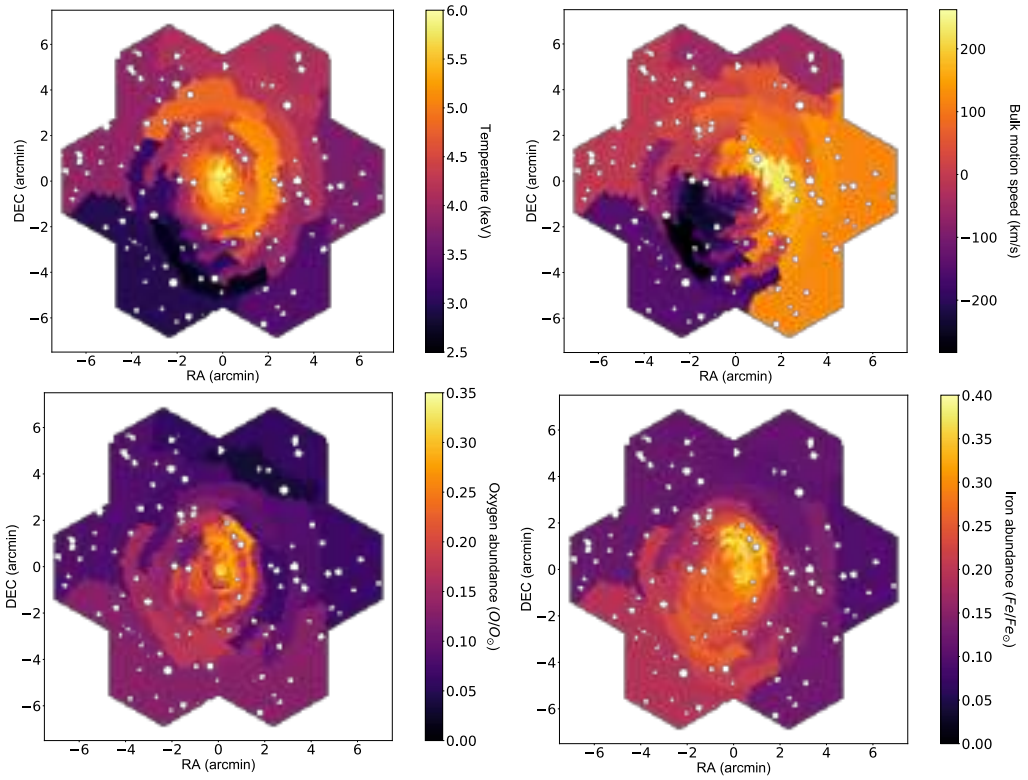

Figure 2 – Physical parameter maps reconstructed from seven 100ks X-IFU observations of a galaxy cluster over regions of S/N 300 (90,000 counts), simulated using the instrument end-to-end simulator SIXTE. The cluster is located at z=0.1, with R500 = 1.1 Mpc and T500 = 4.2 keV, and represents the C2 cluster shown in Figure 1. The image is taken from Cucchetti et al. (2018). From top left to bottom right: The spectral-like temperature (keV), the bulk velocity deduced from line-shift with respect to the cluster average redshift (km/s), and the emission-measure-weighted oxygen and iron abundances (with respect to solar, as per Anders & Grevesse (1989)).

star formation history of the galaxies in the cluster can also be gleaned from the evolution of abundance ratios across time.

The exceptional spectral resolution of the X-IFU will allow accurate abundance ratios to be determined to high redshift ($z > 1$) for the first time (see Fig. 3). An example application is the measurement of the evolution of the ratios of O/Fe and Si/Fe for an ensemble of clusters. This will allow discrimination between models where recent enrichment is caused by SNIa ejection, which produces relatively more Fe than O and Si at low redshift, and models where the enrichment is due to stripping of already pre-enriched member galaxies, which do not show evolution in redshift.

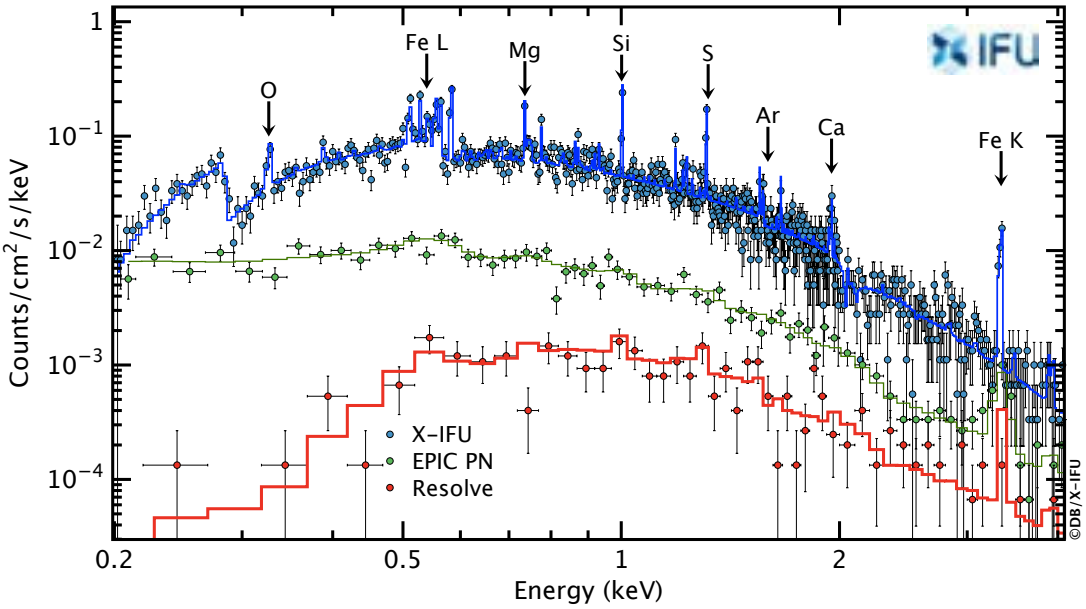

Figure 3 – Simulated X-IFU spectrum of a $z = 1$ galaxy group with $kT = 3$ keV and $L_X = 1 \times 10^{44}$ erg s^{-1} for 150 ks (the normalization of the model is 6.1×10^{-5}). Abundances are set to Solar. The column density is assumed to be 2×10^{20} cm^{-2}. Emission lines from elements which are key to understand chemical evolution can be clearly seen.

From a test sample of four clusters extracted from cosmological hydrodynamical simulations, Cucchetti et al. (2018) presented a set of comprehensive synthetic observations of these clusters at different redshifts (up to z = 2) and within the scaled radius R_{500} performed using the instrument simulator SIXTE (Wilms et al. 2014). Through 100 kilosecond exposures, Cucchetti et al. (2018) demonstrated that the X-IFU will provide spatially-resolved mapping of the

ICM physical properties with little to no biases (<5%) and well within statistical uncertainties. They showed that the detailed study of abundance profiles and abundance ratios within R_{500} provide constraints on the various enrichment models. From synthetic observations out to z = 2, the ability to track the chemical elements across cosmic time with excellent accuracy was demonstrated, enabling to investigate the evolution of metal production mechanisms as well as the link to the stellar initial mass-function.

The heavy elements are ejected and redistributed into the ICM by a number of processes, including outflows and jets from active galactic nuclei, e.g. Kirkpatrick et al. (2011), galactic winds and starbursts, e.g. Strickland & Stevens (2000)), and ram-pressure stripping of the galaxies, e.g. Schindler & Diaferio (2008); in addition, it is also possible that intracluster stars may also contribute to the ICM enrichment, e.g., Gal-Yam et al. (2003).

Spatially-resolved measurements such as abundance profiles provide insight into the different enrichment mechanisms and their spatial distribution, their timescales, and how the gas is mixed by gas-dynamical processes. Detailed abundance mapping is a powerful tracer of the jet energy distribution and can supply constraints on entrainment of enriched gas by the jets, the jet power itself (which is correlated with the radial range of the metal-enriched outflows). It can also put strong constraints on gas physics through ram-pressure stripping of enriched plasma from infalling sub-clumps. The X-IFU will enable all of these measurements to be obtained to unprecedented precision and representative spatial scales.

3.3 AGN feedback on cluster scales

Active galactic nuclei (AGN) at the centres of galaxy groups and clusters play a critical role in shaping the properties of the central galaxy and the surrounding ICM. Mechanical feedback from AGN jets is thought to be one of the best candidates for suppression of star formation in the massive central galaxies and for heating the gas inside and beyond the cluster core. Observations of X-ray cavities surrounding radio lobes in systems from massive elliptical galaxies to galaxy clusters provide observational support for the existence of feedback from AGN jets at all scales, e.g. Boehringer et al. (1993); McNamara et al. (2005).

In the centre of bright, nearby clusters, X-IFU measurements of the X-ray line profiles and variations of the line centroid will allow estimation of the characteristic spatial scales of the turbulent motions induced by AGN jets on scales of tens of kpc, and mapping of the velocity field of the hot gas to an accuracy of $\sim 20\,\mathrm{km\,s^{-1}}$. This will give unprecedented insights into how power from the initially highly collimated jets is distributed into the surrounding ICM. The thermal and non-thermal energy content of the X-ray cavities will be measured accurately for the first time, helping

to establish their composition. X-IFU will help to detect directly the shocked gas surrounding expanding radio lobes, with a spectral resolution sufficient to resolve shock expansion speeds for the first time.

The dynamics of the hot gas in the vicinity of cool filaments will yield essential clues to the cooling and mixing process, and enable for the first time a measurement of the amount of material cooling out of the hot phase and relate this to the fuel available to power the AGN. The X-IFU will enable understanding of the entire cycle of heating and cooling in the cores of nearby clusters and groups. Robust jet power measurements for large samples will be compared to accretion rates of hot and cold material, enabling insights into the accretion process and black hole growth to be obtained.

3.4 The Warm-Hot Intergalactic Medium

The number of visible baryons in the local ($z < 2$) Universe (stars, cold atomic gas and molecular gas in galaxies) adds up to only about 15% of the total number of baryons inferred through a number of independent measurements of cosmological parameters, and recent radio observations have shown the evidence that these, invisible, baryons mostly reside in the gaseous phase. However, not only the detailed state of the baryons remains unclear, but at least half of these baryons are still elusive, and thought to lie in a tenuous web of warm-hot intergalactic medium (the WHIM). X-IFU studies of WHIM will provide unprecedented information on the hot phase of the baryons in large scale structures, complementing the COS/HST observations which are sensitive to the luke-warm phase at $10^{(5-5.5)}$ K.

X-IFU will pursue three independent approaches to the problem:

- Studies of WHIM in absorption against bright AGN at $z < 0.5$, probing low-z LSS and their interplay with the surrounding intergalactic medium;
- Studies of WHIM in absorption (and simultaneously in emission at $z < 0.1$) against Gamma-Ray Burst (GRB) afterglows, probing the WHIM up to redshift of ~ 2 or higher and strongly constraining the physics (i.e., density and temperature) and kinematics (turbulence and bulk motions) of the WHIM for those filaments detected both in emission and absorption;
- WHIM in emission in the outskirts of galaxy concentrations, probing the kinematics of the warm-hot gas near large structures.

The main advances compared to previous instrumentation are the unique combination of large collecting area and spectral resolution. Accurate simulations based on theoretical predictions, show that the X-IFU will be able to fully understand the WHIM baryon budget with a set of ~ 40 Athena observations of bright nearby ($z < 0.5$) AGN and more distant ($z < 2$) GRB afterglows.

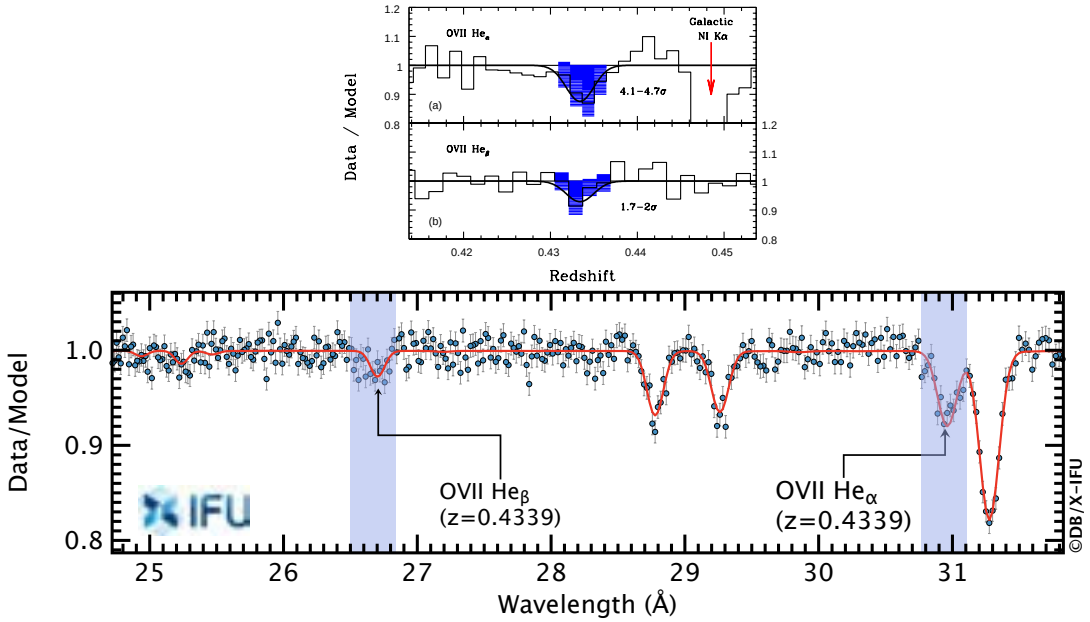

Figure 4 – Top) XMM-Newton RGS spectrum showing the absorption line of an intervening absorber at z= 0.3551 (Nicastro et al. 2018). Bottom) Simulated X-IFU spectrum of the same absorber. The plots shows the ratio of the X-IFU data of the blazar 1ES 1553+113 with the local best-fitting continuum model, to highlight the two OVII He-α and He-β absorption lines. The simulation is performed with the response matrix of the X-IFU in which the spectral resolution at 1 keV is about 2.1 eV. The integration time is 160 kseconds, consistent with the observation listed in the Mock Observing Plan (v4). The XMM-Newton RGS observation from which the simulation is derived was 1.75 Ms long.

Recently the detection of two absorbers of highly ionized oxygen (OVII) in the X-ray spectrum of a quasar at a redshift higher than 0.4 was reported from a 1.7 Ms long observation of XMM-Newton RGS (Nicastro et al. 2018), leading to the conclusions that the missing baryons had been found. The advances permitted by the X-IFU are illustrated in Figure 4 where a simulation of 160 kilo-second observation is compared with the 1.75 Ms long RGS spectrum. Clearly the signal-to-noise ratio of the line is considerably increased despite the integration time of the observation being an order of magnitude shorter.

4 The Energetic Universe

X-IFU observations will measure the energy released by accretion onto black holes by winds and outflows from the local Universe all the way up to $z \sim 3$, providing

solid ground to understand AGN feedback. In nearby galaxies, the amount of gas, energy and metals blown into the circum-galactic medium by both AGN and starbursts will be mapped. By targeting distant GRB afterglows, X-IFU observations will characterise the ambient interstellar medium of high-z galaxies and constrain their prevailing stellar populations. Deep X-IFU observations of distant AGN will be able to unveil their redshift via the Fe K emission line and characterize their outflows up to $z \sim 3-4$.

4.1 High-z Gamma-ray Bursts: early metal enrichment of the Universe

X-IFU observations of gamma ray bursts can play a unique role in the study of metal enrichment as GRBs are the brightest light sources at all redshifts and, for long duration events (LGRBs), occur in star-forming regions. As LGRB progenitors are short-lived massive stars, they provide an ideal probe of the effect of stellar evolution on galaxy chemical enrichment across cosmic time. Beginning with metal free (Population III) stars, the cycle of metal enrichment started when their final explosive stages injected the first elements beyond Hydrogen and Helium into their pristine surroundings, quickly enriching the gas. These ejecta created the seeds for the next generation of stars (population II). Finding and mapping the earliest star formation sites (population III/II stars) is one of the top priorities for future astrophysical observatories. Tracing the first generation of stars is crucial for understanding cosmic re-ionization, the formation of the first seed Super-Massive Black Holes (SMBH), and the dissemination of the first metals in the Universe. Photons from Pop III stars and radiation generated from accretion onto the first SMBH initiate the Cosmic Dawn.

The chemical fingerprint of Pop III star explosions is distinct from that of later generations, opening the possibility to probe the Initial Mass Function (IMF) of the Universe. Stellar evolution studies show that the nucleosynthetic yields of Pop III and Pop II explosions differ significantly. The convolution of these yields with an IMF directly translates to abundance patterns, which can differ up to an order of magnitude depending on the characteristic mass scale of the IMF (Heger & Woosley 2010). The X-IFU will be able to measure metal abundance patterns for a variety of ions (e.g., S, Si, Fe) for at least 10 medium-bright X-ray afterglows per year with H equivalent column densities as small as $10^{21}\mathrm{cm}^{-2}$ and gas metallicities as low as 1% of solar for the denser regions expected in early star-forming zones; in even denser regions the accuracy will be further improved (Fig. 5). Measuring these patterns using GRBs, combined with Athena studies of AGN sightlines, galaxies and supernovae, will enable us to determine the typical masses of early stars, thereby testing whether or not the primordial IMF is indeed top heavy, see

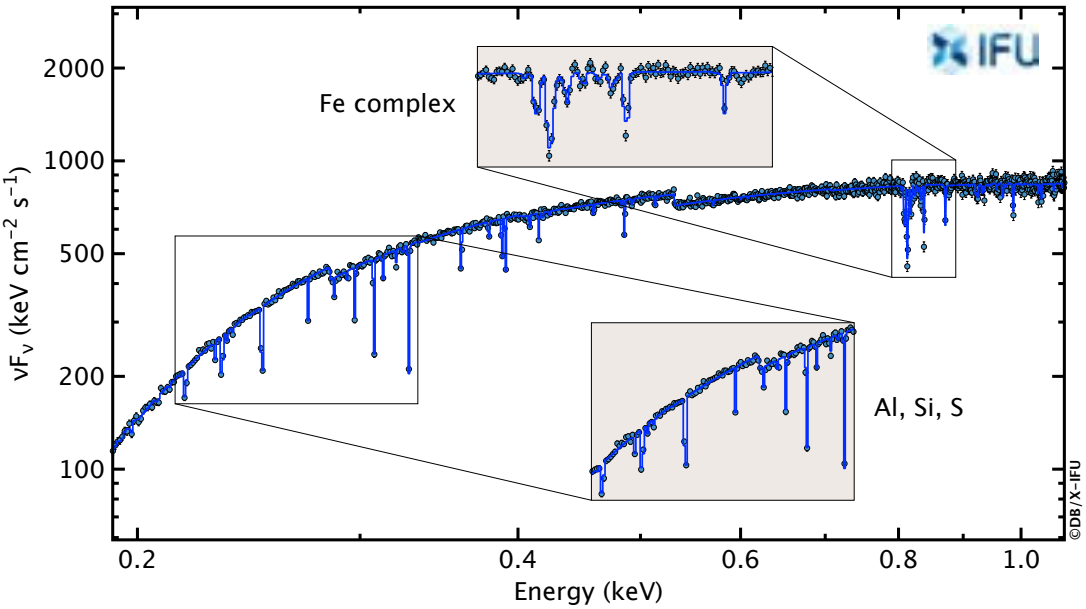

Figure 5 – A simulated X-IFU X-ray spectrum of a medium bright (fluence = 0.4×10^{-6} erg cm^{-2}) afterglow at $z = 7$, characterized by deep narrow resonant lines of Fe, Si, S, Ar, Mg, from the gas in the environment of the GRB. An effective intrinsic column density of 2×10^{22} cm^{-2} has been adopted.

Jonker et al. (2013a) for more information.

4.2 AGN and Star-formation driven winds and outflows

The measurement of tight correlations between the mass of galaxy bulges, or of the velocity dispersion of their stellar content, and the mass of the SMBH hosted in all galaxies (Kormendy & Richstone 1995; Magorrian et al. 1998) strongly indicate that some feedback mechanism must have acted between these components during the galaxy formation and evolution phases. In the last fifteen years, thanks to X-ray observations of quasars and nearby Seyfert galaxies, we have been able to identify AGN driven ultra-fast outflows (UFOs) as one of the plausible mechanisms (Chartas et al. 2002; Pounds et al. 2003; Tombesi et al. 2010a). UFOs manifest themselves as blueshifted resonant absorption lines due to highly ionized iron. They are detectable in the 7-10 keV band (Tombesi et al. 2010a,b) and are thought to be related to winds that are energetic enough to quench the star formation of the host galaxies. This provides the link between the tiny SMBH and the huge galaxy bulges (Tombesi et al. 2015), see King & Pounds (2015) for a review on this topic. However, we still lack some fundamental pieces of evidence to fully

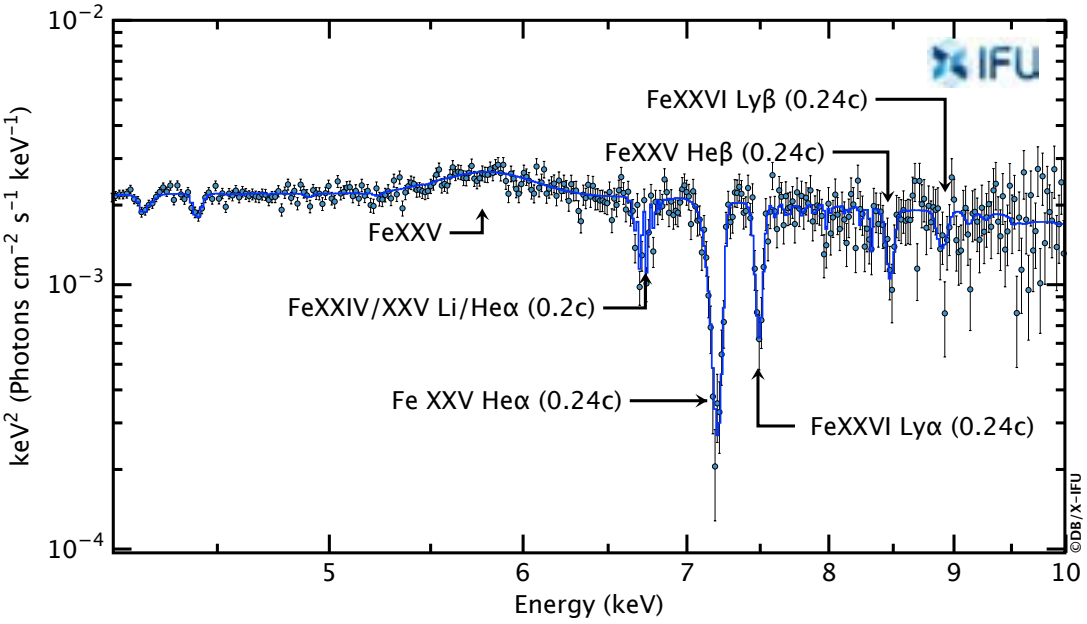

Figure 6 – Simulated 100 ks X-IFU spectrum of PDS456 ($z = 0.184$) above 4 keV obtained assuming a source state as in the XMM+NuSTAR observations of PDS456 as shown in Reeves et al. (2018). We assumed here a soft X-ray absorber with a turbulence velocity of 300 km/s and an ultra fast wind component with a turbulence velocity of 3000 km/s. The soft wind has a column density of $\sim 2 \times 10^{22}$ cm^{-2} and ionization of $\log \xi = 3.1$ and is outflowing with $v \sim 0.2c$. The ultra fast wind has a column density of $\sim 1.5 \times 10^{23}$ cm^{-2}, $\log \xi = 3.6$ and $v_{out} \sim 0.24c$.

verify this scenario: 1) we do not know what is the launching mechanism of the UFOs, how they deposit their energy into the interstellar medium and how they interact with star forming regions; 2) we have only poor knowledge of the physical conditions of the AGN engine and of the importance of UFOs at high-z, i.e., in epochs where both QSO and starburst activity were at their highest (Boyle et al. 1988; Madau et al. 1996; Brandt & Hasinger 2005, and references therein).

To investigate the first of the above mentioned questions, we should obtain a detailed characterization of the physical properties of UFOs (column density, ionization state, outflow velocity, location, geometry, covering factor, etc.) and check how they evolve with respect to the distance from the source, maximum outflow velocity, and X-ray or UV luminosity (see Fig. 6). We must also consider that UFOs are known to be variable (Tombesi et al. 2015) and so we must be able to investigate the above mentioned properties on time-scales of $\approx 10 - 100$ ks (corresponding to the dynamical time-scale at $10\,R_g$ for a SMBH with $M \sim 10^{7-8} M_\odot$). The coupling of the large collecting area and of the exquisite energy resolution of X-IFU provides

the capability to perform such kind of studies (Cappi et al. 2013) on a sample of at least $\sim 50-80$ nearby ($z < 0.01$) and bright ($F_{2-10\,\mathrm{keV}} > 10^{-11}\,\mathrm{erg\,cm^{-2}\,s^{-1}}$) Seyfert galaxies with the accuracy needed to disentangle the right scenario among the radiation-driven, e.g. Proga & Kallman (2004); Sim et al. (2010), momentum-driven (King 2010), and magnetically-driven (Fukumura et al. 2010) accretion disc wind models. Moreover, the ability of the X-IFU to simultaneously obtain high-resolution X-ray spectra and good quality images for nearby galaxies will allow us to investigate where and how the AGN driven winds interact with the interstellar medium, what is the interplay among the AGN- and the starburst-driven winds, and how these winds enrich the intergalactic matter. In this respect it will be important to study nearby starburst and Luminous Infrared Galaxies (LIRG)/Ultra Luminous Infrared Galaxies (ULIRG) with the main goal to map, from good quality X-ray spectra, regions dominated by collisionally-ionized plasmas (hot gas), non-equilibrium ionization (shocks) and photo-ionized plasmas. Within its nominal life, X-IFU will be able to obtain such information for at least 30 objects thus allowing, for the very first time, to have a clear vision of such phenomena in the nearby Universe.

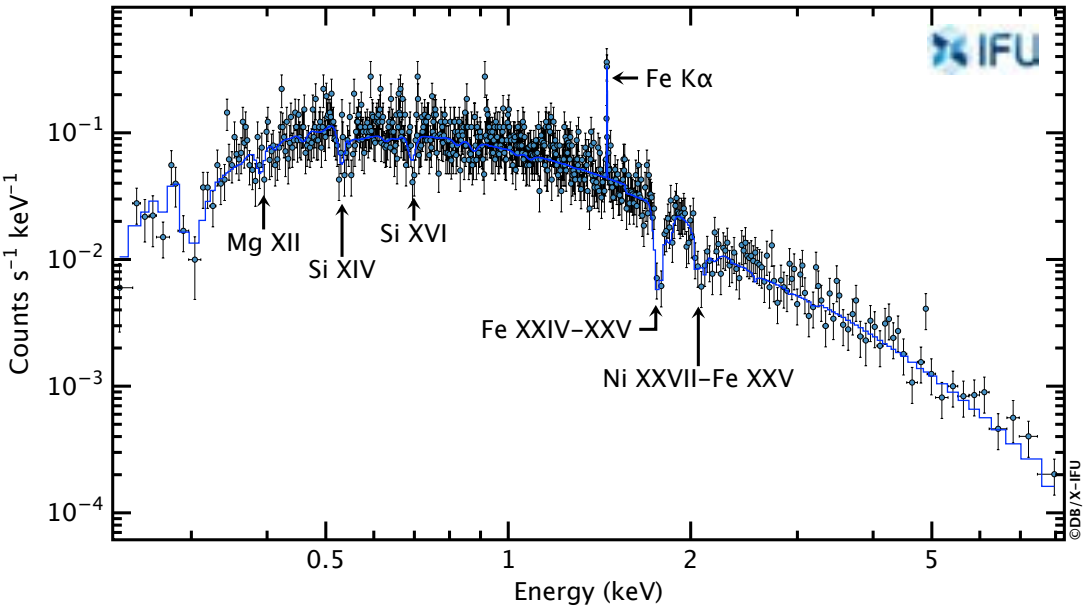

Figure 7 – Simulated Athena X-IFU 50 ks spectrum for a hyper-luminous quasar at z = 3.4 with an UFO absorber with velocity 0.15c, NH=$10^{23.4}$ cm^{-2}, log(U) = 2.3 and a turbulent velocity of 5000 km/s (Martocchia et al. 2017). The solid line indicates the best-fit baseline continuum model modified by the UFO and the Fe Kα line. Prominent absorption lines with observed equivalent width > 1 keV and the Fe Kα emission line are shown.

To fully understand if and how these winds acted along cosmic time to shape the SMBH-galaxy co-evolution, we must finally couple the knowledge on the launch and SMBH-host galaxy interaction mechanisms obtained at low redshift with a reliable census of the UFOs and of their properties at high-z, i.e., we must answer the second of the above mentioned questions. Up to now, UFOs have been measured only in a handful of mostly lensed (i.e., brightness enhanced) QSO at high redshift (Chartas et al. 2002, 2003, 2007; Lanzuisi et al. 2012; Vignali et al. 2015). This clearly demonstrates that the capability to collect photons is fundamental to obtain the information we need. The Athena collecting area will enable investigations of the properties of ionized and outflowing absorbers in large samples of QSO ($L_{\rm X} \geq 10^{44}\,{\rm erg\,s^{-1}}$) up to redshift $z \sim 4$ (Georgakakis et al. 2013; Martocchia et al. 2017) (see Fig. 7). Moreover, the wide angle surveys performed using WFI will produce rich samples of hundreds of QSO suitable for detailed spectroscopic studies with the X-IFU. These studies are expected to allow reliable estimates of the physical parameters of UFOs at the knee (L^*) of the X-ray luminosity function, which dominate the growth of SMBH at $z \sim 1-4$. We expect to be able to fully test the scenarios that assume the AGN driven winds as the mechanism to self-regulate the star-formation and SMBH growth along cosmic times.

Recently Dadina et al. (2018) reported the first detection of an UFO in a radio-loud quasar at $z \geq 1.5$. The signature of the UFO is an absorption line at 9.2 keV redshifted to 2.5 keV, interpreted as due to FeXXVI, implying gas outflowing at $\sim 0.3c$. Estimates of the involved energetics suggest that such UFOs are powerful enough to impact on the evolution of the host galaxies. This result adds support to evidence that the rate of UFOs in high-z quasars is rather large. X-IFU will routinely probe UFOs near the peak of AGN activity (in short exposures), thus enabling 1) to test feedback models in which UFOs may quench the star formation in their host galaxies, 2) to determine their contribution in shaping the $M-\sigma$ relation, and 3) to determine the powering mechanism of UFOs (e.g. magnetic field driving the outflows).

4.3 Super massive black hole spins

Thanks to its high energy resolution and sensitivity, the X-IFU will allow the measurement of SMBH spins with unprecedented accuracy in a large number of AGN even beyond the local Universe.

The angular momentum is, in addition to mass, the other fundamental parameter that characterizes astrophysical black holes and therefore a proper census of SMBH in the Universe requires the measurement of their spins. This is also

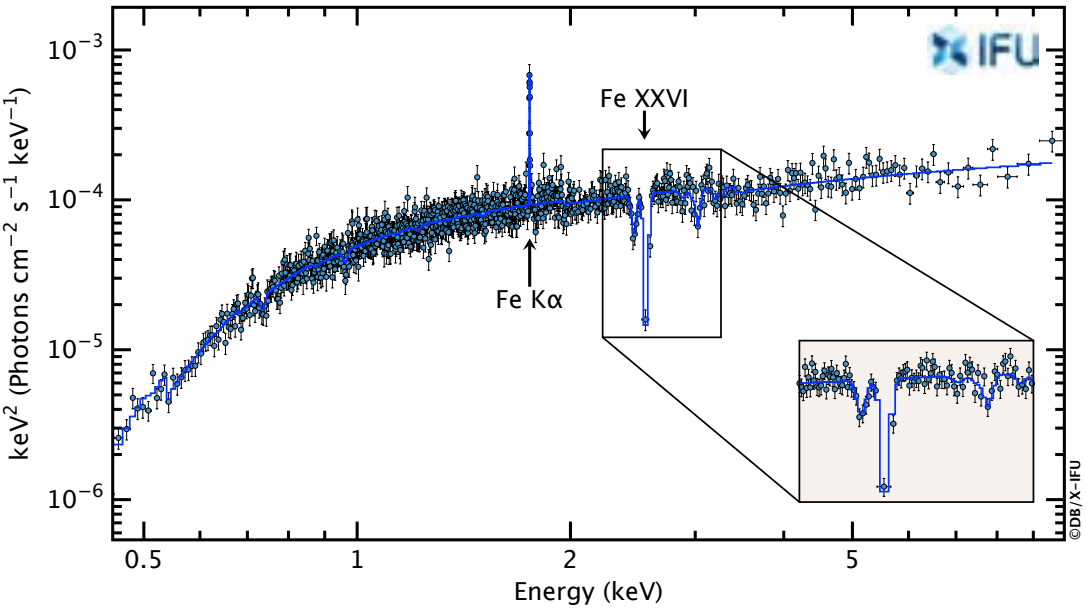

Figure 8 – Simulated 50 ksecond X-IFU observed frame energy spectrum of MG J0414+0534 (a QSO at z=2.64) based on a model consisting of warmabs model based on Xstar (Dadina et al. 2018). The outflow velocity is set to 0.28 c. The ionization state ($\log(\xi) \sim 4$) implies that that the absorption line is likely due to FeXXVI. A narrow Fe K α line is also present in the system.

of fundamental importance in order to understand the black hole growth history (Berti & Volonteri 2008), particularly the relative roles of mergers and chaotic accretion, that tend to reduce the spin, versus prolonged accretion, that generally increases it. Moreover a systematic study of SMBH spins would shed light on the relation between SMBH rotation and its outflow power in the form of relativistic jets. Since the influence of the spin is felt only up to a few gravitational radii, X-ray observations, probing the innermost regions of SMBH systems, are the main tool for such measurements.

The simplest and most widely applicable way of measuring SMBH spins is via time-averaged spectral fitting of relativistically broadened Fe Kα lines (Fabian et al. 2000). The larger the spin, the closer to the horizon will be the innermost stable circular orbit (ISCO) of a prograde accretion disk resulting in a larger broadening and skewing to the red of the reflected lines. Broad lines are present in at least $\sim 30-40\%$ of bright nearby type 1 AGN (Nandra et al. 2007; de La Calle Pérez et al. 2010) and reliable estimates of SMBH spins have already been made in about 20 AGN with this technique, e.g Reynolds (2014); Brenneman (2013); Risaliti et al. (2013); Walton et al. (2013). The Fe line is always accompanied

by a reflection continuum in hard X-rays and, if the reflecting matter is at least partly ionized, also in the soft X-rays. With its large effective area over a broad energy range X-IFU will permit the simultaneous use of the iron line and of the soft X-ray reflection continuum to measure black hole spins also at intermediate redshifts. As an example, the spin of a maximally rotating black hole in PB5062, a luminous ($L_{\rm X} \sim 2 \times 10^{45}\,{\rm erg\,s^{-1}}$, 2-10 keV) QSO at $z = 0.532$ (Kammoun et al. 2017) can be recovered with a precision of 20% in a 100 ks observation.

One of the difficulties in these measurements is to disentangle the different AGN spectral components that come from regions at different distances from the SMBH. With its excellent energy resolution the X-IFU will easily separate the broad emission and absorption lines from the narrow features, which are ubiquitous in AGN and originate from more distant matter (Yaqoob & Padmanabhan 2004) and this will again allow to increase drastically the sample of measured SMBH spins.

X-IFU will also be able to map the inner regions of the accretion disks in the time-energy plane. Any deviation from axial symmetry in the disk emissivity (e.g., associated with hot spots) will lead to a characteristic variability of the iron line Dovčiak et al. (2004), with arcs being traced out on the time-energy plane (Armitage & Reynolds 2003). Evidence of hot spots were found in XMM-Newton data (Iwasawa et al. 2004; de Marco et al. 2009) and they are of great diagnostic power for tracing the inner turbulent flow of the disk in the strong gravity environment. General Relativity makes specific predictions for the arc forms and from a fit of these features one can derive SMBH mass and spin as well as the disk view inclination.

4.4 Accretion physics

Outbursts from Galactic stellar-mass black holes and neutron stars span orders of magnitude in mass accretion rate, and evolve over days, weeks, and months (Remillard & McClintock 2006; Dunn et al. 2010; Reynolds & Miller 2013). In contrast, the same dynamic range in AGN is not accessible on human timescales. The high flux observed from Galactic sources ensures very high sensitivity in the crucial Fe K band, wherein the most highly ionized gas –likely tied to the region closest to the black hole– is observed. Discoveries made in the Fe K band in stellar-mass black holes help to direct and sharpen subsequent observations of AGN. In short, Galactic compact objects represent rapidly evolving, high-flux proxies that are vital to understanding the much larger classes of Seyfert galaxies and quasars.

Theoretical studies demand that black holes must be fuelled by accretion disks wherein magnetic processes mediate the transfer of mass and angular momentum (Shakura & Sunyaev 1973; Blandford & Payne 1982; Balbus & Hawley 1991). In addition, the angular momentum can be transported throughout the accretion flow

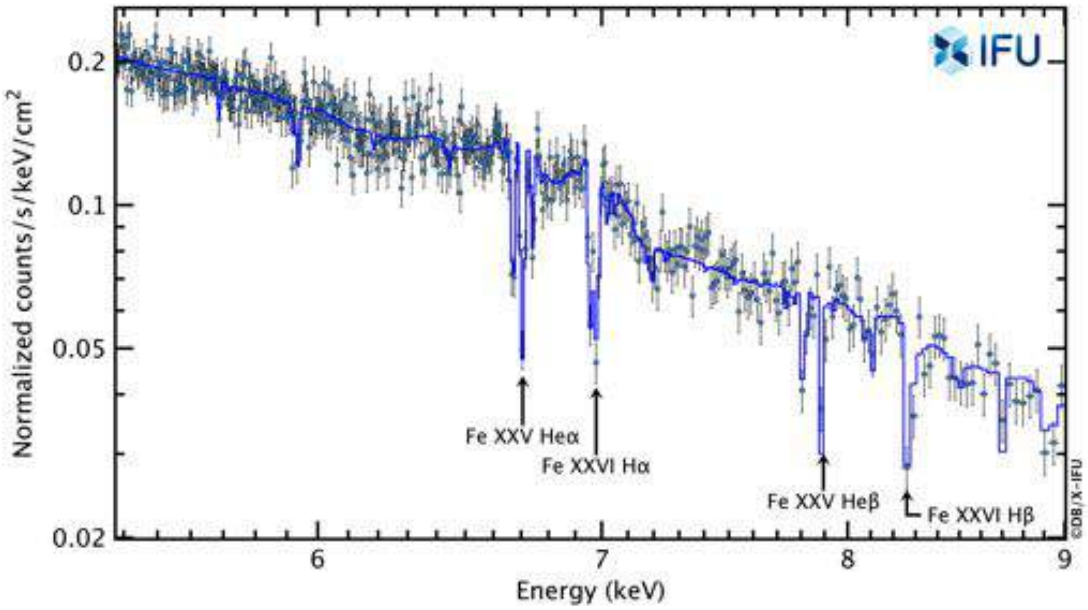

Figure 9 – X-IFU simulated observation lasting only $\sim$ 120 seconds of the Black Hole binary GRS1915+105. A disk wind, as reported in Miller et al. (2016) has been simulated. Strong spectral features can be clearly seen in the spectrum, including Fe XXV Kα (6.65 – 6.75 keV), the resolved doublet Fe XXVI Kα (6.95 – 7.00 keV), Fe XXVI Kα shifted by 0.01c (7.00 – 7.05 keV), Fe XXVI Kα shifted by 0.03c, Fe XXV Kβ (7.65 – 7.90 keV) and Fe XXVI Kβ (8.20 – 8.35 keV). This rich set of features will enable unprecedented studies of the structure of the disk winds.

via the non-axisymmetric waves and shocks, related to the self-gravitating parts of disks in active galactic nuclei, or to the regions tidally excited by the companion star in black hole binaries (Fragile & Blaes 2008).

For decades, one were only able to observe the effects of the fundamental disk physics (thermal spectra, jet ejection episodes), but unable to probe the underlying process that fuels black holes in Seyfert and quasar accretion modes. Very new observations may now indicate that disk winds can be used to constrain the emergent magnetic field of accretion disks (Miller et al. 2016). This opens a long-awaited window on the fundamental physics of disk accretion and enables connections to numerical simulations. This is also a window on mechanical feedback from black holes, since feedback modes may depend on the disk magnetic field strength and configuration (Livio et al. 2003; Begelman et al. 2015).

Equipped with the X-IFU, Athena will have the power to reveal the fundamental physics that drives accretion onto black holes. The keys are spectral resolution, and sensitivity. Whereas current telescopes can only offer initial constraints on disk

physics in 100 kilo-seconds, the X-IFU will be able to constrain magnetic fields via winds in just hundreds of seconds - the dynamical time scale of such winds. The evolution of the outflow properties (mass outflow rate, kinetic power) and disk fields will finally be accessible on their natural time scale (see Fig. 9).

Jets may be the main agents of feedback from black holes into environments as large as galaxy clusters. In both stellar-mass black holes and AGN, momentary dips in the X-ray flux have been associated with relativistic jet ejection events (Belloni et al. 1997; Chatterjee et al. 2009, 2011). These dips last 100s of seconds in stellar-mass black holes. Whereas prior missions have only been able to observe continuum variations that do not reveal velocities or accelerations, X-IFU will be able to obtain sensitive line spectra as mass is transferred from the disk into the jet, providing a new and unparalleled view of the jet launching process.

For black holes that accrete at rates more than a few per cent of the Eddington limit, the inner region of the flow will be dominated by radiation rather than gas pressure Lightman & Eardley (1974). Observationally, two microquasars have shown spectacular X-ray variability on timescales of order of 50-100 s, that confirm the limit-cycle nature of the underlying process (Belloni et al. 2000; Altamirano et al. 2011). Moreover, the observed interplay between the wind outflow launched in some states of the sources and such 'heartbeat' variations has shed some light on the plausible disk stabilizing force (Janiuk et al. 2015). The magnetic fields, or, in general, the intrinsically stochastic nature of the turbulent dissipation must be an important agent here (Janiuk & Misra 2012). X-IFU observations of these and other targets will reveal to exquisite detail the structure of these winds and allow a detailed study of disk wind launching mechanisms and open a window into the study of fundamental disk physics.

4.5 Sgr A*

A remarkable case that links the stellar BH to the SMBH of AGN is the massive BH at the center of our own galaxy, Sgr A*. With its 4×10^6 $M_\odot$ mass and consequently a time scale of $\sim$ 30 min at the ISCO, its clean close environment due to the low accretion rate and the fact that it is relatively nearby, Sgr A* offers the opportunity to study the details of its steady accretion flow and the non-thermal flares that take place within a few Schwarzschild radii from the horizon. Even if challenging because of the confusion in the inner 5" of the galaxy, the X-IFU will allow to study the spectral lines of the Sgr A* accreting plasma (Wang et al. 2013) providing insights in the physical conditions and dynamics of the flow. X-IFU will also be able to explore in detail the variable fluorescent spectral lines from the molecular clouds of the central zone which are reflecting radiation from ancient outbursts of the BH (Ponti et al. 2013; Clavel et al. 2013). With its excellent spectral-imaging performances the X-IFU will obtain Molecular Cloud line diagnostics unreachable

to present instruments and crucial for the reconstruction of Sgr A* light curve in the past 1000 yr, probing the link between dormant SMBH and their past active phases.

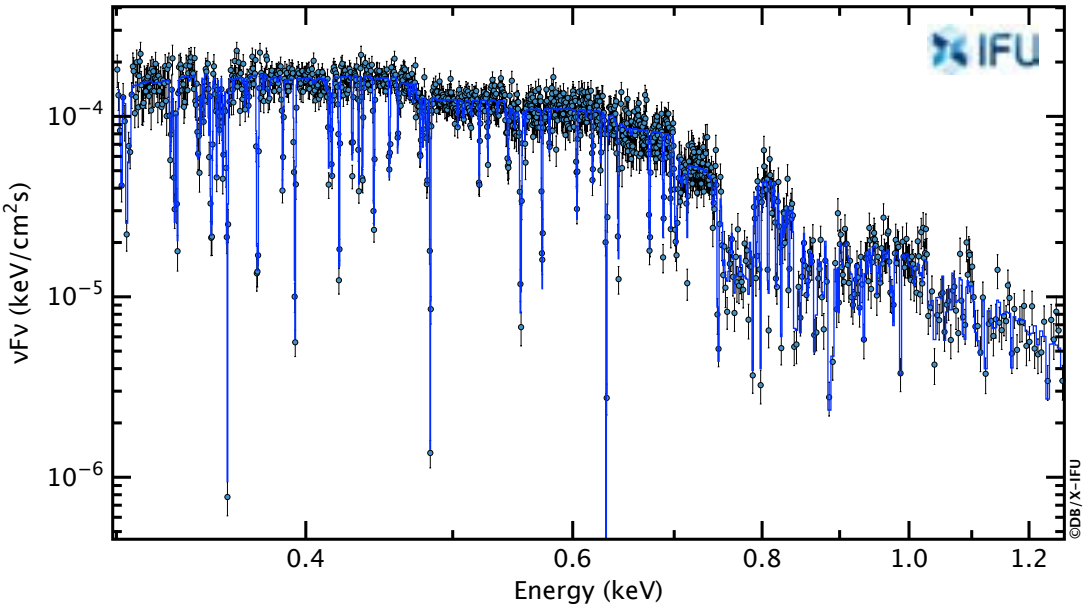

Figure 10 – The simulated spectrum of a TDE event like 3XMM J152130.7+074916 (Lin et al. 2015). With such a spectrum, it is possible to measure sub-relativistic absorbing outflows from tidal disruption events in the peak. It is expected that at the peak of tidal disruption events, the accretion rates could exceed the Eddington limit, in which case strong outflows would be common and absorb the spectra. The resulting very rich absorption lines can be used to probe the properties of the outflow in such extreme environments. Data are courtesy of Dacheng Lin.

4.6 Tidal Disruption Events

Tidal disruption events (TDEs), long lived events, in which stars are tidally disrupted and subsequently accreted by massive black holes (BHs) at the centre of galaxies can reveal an otherwise dormant supermassive black holes in galactic nuclei, see e.g. Jonker et al. (2013b) and references therein. TDEs may also reveal the presence of intermediate mass black holes (Lin et al. 2018); a family of black holes that may help explaining the presence of super-massive black holes early in the Universe. The X-ray spectra of TDEs are generally soft and can be described with Comptonized emission from an optically thick low-temperature corona, a super-Eddington accretion signature often observed in accreting stellar-mass black

holes, e.g. Lin et al. (2015). A key feature of super-Eddington accretion disks is a lower radiative efficiency than a standard thermal thin disk, due to significant super-Eddington effects of photon trapping and powerful sub-relativistic winds, which may be revealed through absorption lines in high resolution X-ray spectra. The X-IFU will probe these winds thus providing unique information on the mass outflow rate energetics (see Figure 10).

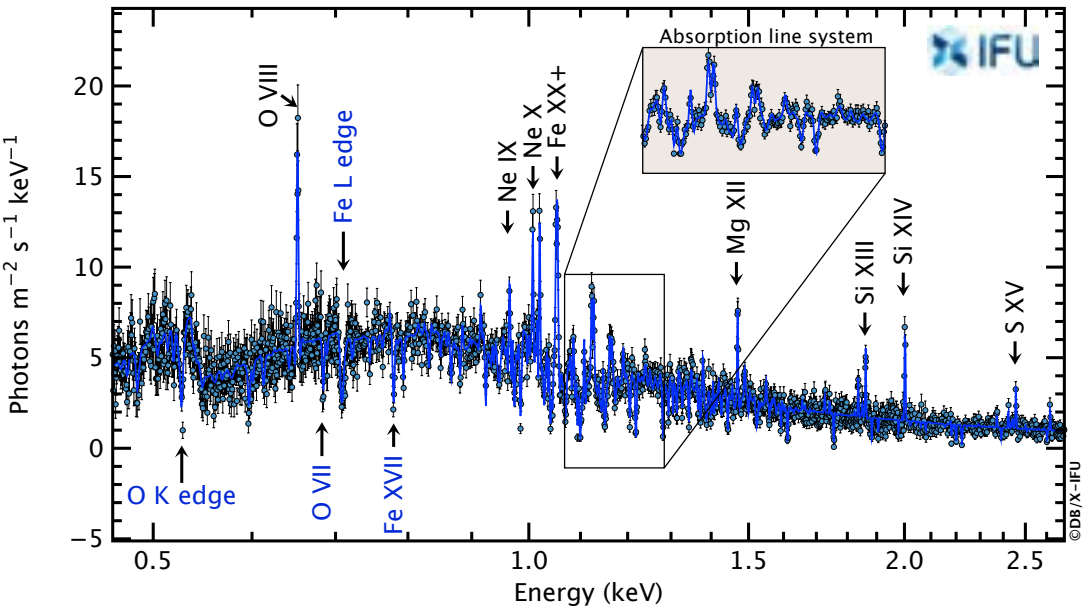

Figure 11 – Simulated Athena X-IFU 25 ks spectrum for the archetypal ultra-luminous X-ray source NGC 1313 X-1. The spectral model is a power-law ($\gamma = 1.9$ and $L_{0.3-10keV} = 10^{40}$ erg/s) absorbed by an ultra-fast outflowing gas in photoionization equilibrium with velocity $0.19c$, $N_H = 10^{22}$cm^{-2},log(ξ) = 2.34 and turbulent velocity of 500 km/s (FWHM). The emission lines are produced by a collisionally-ionized equilibrium plasma model with T=1.3 keV (the temperature of the collisionally-ionized gas) and $L_{0.3-10keV} = 10^{39}$ erg/s (solar abundances are adopted for both the absorbing and emitting gas, see Pinto et al. (2016)). Prominent blueshifted absorption and rest-frame emission lines are shown. Data are courtesy of Ciro Pinto.

Super-Eddington accretion may contribute significantly to the production of super-massive black holes. Studying super-Eddington accretion is possible through the observation of ultra-luminous X-ray sources (ULXs), off-nuclear sources exceeding the Eddington limit for 10 solar-mass black holes. Super Eddington winds have now been detected from a handful of ULXs, see e.g.

Pinto et al. (2016). As shown in Figure 11, the X-IFU will probe super-Eddington winds with exquisite details, thanks to a perfect combination of throughput and spectral resolution. Multiple emission and absorption lines will be detected so that the total mass outflow rate and kinetic power of the wind can be measured. X-IFU will open the way to observation of super-Eddington outflows on short timescales, providing insights on the physical processes that make them transient or variable in other systems, e.g. the AGN UFOs discussed above.

5 Observatory science

While focusing on the Hot and Energetic Universe, the breakthrough capabilities (e.g., excellent spectral resolution combined with high throughput and fast timing capabilities) of the X-IFU will enable a wealth of new science investigations to be performed for a wide range of astrophysical sources of great interest to the broader astronomical community. This so-called observatory science covers very different topics and we highlight here only a few of them. We also highlight the potential of X-IFU observations in unforeseen discoveries thanks to the Athena fast Target of Opportunity observation capability, in particular in science triggered by new Gravitational Wave detectors.

5.1 Solar system and planetary science

Athena investigations of the solar system will answer questions still open following the pioneering work carried out with Chandra and XMM–Newton, and will add enormously to our understanding of the interactions of the solar wind with planetary bodies, and between space plasmas and magnetic fields. The X-IFU will determine the species, and thus the origin (solar wind or Io's volcanoes), of the ions responsible for Jupiter soft X-ray aurora, and will test theories of ion acceleration in the planet magnetosphere through line broadening velocity measurements (see Fig. 12). High sensitivity observations of X-ray fluorescence from the Galilean moons will allow surface composition measurements, and studies of the Io plasma torus will shed light on the yet unknown mechanisms energizing its X-ray emission. A search for X-ray aurorae on Saturn with the X-IFU will reach much greater depth than possible so far. The X-IFU will spectroscopically map Mars extended exosphere through differing solar wind conditions and seasons, as well as the very extended comae of comets transiting in the Sun neighborhood.

The X-IFU will drastically improve our knowledge of the consequences of X-ray incidence on exoplanets, a crucial element in order to understand the effects of atmospheric mass loss and, more generally, of the chemical and physical evo-

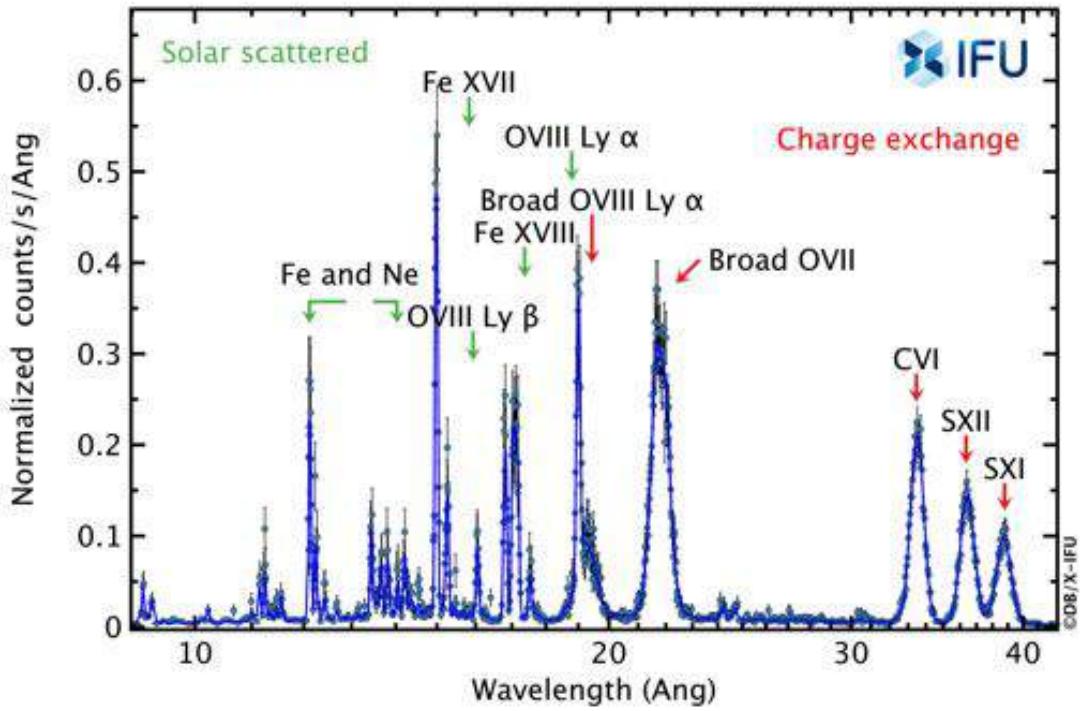

Figure 12 – Simulated Jupiter's spectrum for a 20 kilo-seconds Athena X-IFU observation, showing clearly the emission lines produced by charge exchange between solar wind particles and Jupiter's atmosphere.

lution of planet atmospheres especially in the early evolutionary stages. In a few selected nearby known planetary systems hosting hot Jupiters, X-IFU will search for ingress/eclipse/egress effects during planetary orbits. In a wider sample of planetary systems X-IFU can confirm/improve the statistical evidence of Star-Planet Interactions and search for those variability features that are imprints of such interactions. Athena may also discover unexpected spectral signatures (and their orbital modulation) of planetary atmospheres due to the host stars high energy radiation and particle emission.

5.2 Massive stars

The powerful and energetic stellar winds of massive stars make them key players in mechanical and chemical feedback processes within galaxies, whatever their redshift. However, large uncertainties and discrepancies remain in the quantitative evaluation of the wind properties, impeding a proper understanding of massive star evolution and feedback. X-rays form from hydrodynamic shocks inside these

stellar winds, making them a sensitive probe of the wind properties. Time resolved high-resolution spectroscopy, collected by X-IFU, is especially important in this respect. Indeed, X-IFU will allow to probe for the first time the variability of the morphology and intensity of the X-ray lines of these stars. These studies are beyond the reach of current X-ray spectrometers. The X-IFU data will provide major breakthroughs for various questions related to massive stars, and thus dramatically increase our understanding of the plasma physics in the most important stellar feedback engines (Sciortino et al. 2013).

In single stars, small-scale structures directly linked to the degree of wind inhomogeneity will be probed by quantifying short-term variations as well as overall line profile shapes in a large sample of objects. In addition, detailed Doppler mapping will pinpoint the properties of large-scale structures, notably linked to magnetic confinement or co-rotating features, whose presence could just be hinted at in the best datasets currently at hand, e.g. ud-Doula & Nazé (2016); Nazé et al. (2018). Likewise, studying the variability of X-ray lines in massive stars which display β Cep-like pulsations in the optical and in X-rays (Oskinova et al. 2014; Cazorla & Nazé 2017) will provide unprecedented insight into the connection between the pulsations at the level of the photosphere and the dynamics of the stellar wind.

The majority of the massive stars live in binary or higher multiplicity systems. In massive binary systems, the stellar winds of both stars collide, leading to an additional powerful X-ray emission arising from the wind interaction zone. For such systems, X-IFU will perform the first precise phase-resolved line profile studies, in particular of the Fe XXV line complex near 6.7 keV, thereby yielding the immediate post-shock conditions in the wind interaction zone and allowing direct mapping of the wind interaction via Doppler tomography (Rauw et al. 2016).

5.3 Cool stars

High-energy irradiation of circumstellar disks during star formation and early stellar evolution are crucial for disk evolution and, eventually, resulting planetary system formation (Glassgold et al. 2000). The radiation associated with magnetospheric accretion onto CTTS (Classical T Tauri Stars) and young Brown Dwarfs is believed to originate in localized structures (accretion streams and hot spots). Therefore, the observed emission changes throughout the stellar rotation cycle and the X-IFU will probe the X-ray line emission from the heated plasma in shocks forming upon impact of the accreting matter on the stellar surface, while accompanying simultaneous optical studies will monitor the line emissions produced in magnetic accretion channels. The viewing geometry crucially determines what we see in X-rays as in TW Hya (Brickhouse et al. 2010) and V2129 Oph, (Argiroffi et al. 2011) and the detailed mapping of the accretion geometry, therefore, re-

quires simultaneous optical and X-ray monitoring for at least one rotation cycle, i.e., typically a few days. Spectro-polarimetric optical monitoring (e.g., with E-ELT/HIRES) simultaneous (e.g for at least one night) with X-IFU observations provides both time-resolved emission line fluxes tracing accretion columns and maps of the large-scale magnetic field structure. With X-IFU for the brightest ($F_X \sim 3 \times 10^{-13}$ erg cm^{-2} s^{-}1) CTTSs high resolution time-resolved spectroscopy down to 3 kilo-seconds will allow us i) to explore the variability of the accretion process (on predicted time scales of hours) and/or the modulation due to accretion stream shadowing, ii) to constrain with Doppler line shifts down to 100−400 km s^{-1} the bulk velocity of accreting material, iii) to investigate from simultaneous observations of many density sensitive triplets the controversial issue of density stratification of accreting material, and iv) to address the open and controversial issue of the excitation mechanism of the Fe Kα 6.4 line emitted from the circumstellar disk (Giardino et al. 2007).

Understanding the physics of the early interaction between radiation (and energetic particle streams) and early disk should greatly improve our understanding of planet formation and early evolution. The fluorescent emission is one of the handles as complex physics is at work. The analysis of a recent long joint XMM-Newton and NuSTAR observation of the Class I/II Elias 29 (Sciortino et al. 2018; Pillitteri et al. 2018) has confirmed that the 6.4 keV Fe line is detected during quiescent and flaring states and its flux is variable with an EW ranging from 0.15 to 0.5 keV. The EW values make unrealistic a simple model with a centrally illuminated disk and suggest a role of the cavity containing Elias 29 and possibly reverberation processes that could occur in it. There is evidence (at 95% confidence level) that the centroid of the fluorescent line vary in time (down to the explorable tens of ksec time-scale). This points toward a scenario where the emission arises from excited material at different ionization stages whose relative contributions do vary with time. X-IFU time resolved spectroscopy will be able to confirm the validity of such a scenario and uncover the detailed physics at work for which we still miss a clear understanding (see Figure 13).

Strong flares (peak $L_{\rm X} \sim 10^{32}$ erg s^{-1}, peak $T \sim 2 \times 10^8$ K) on young active stars and the likely associated huge Coronal Mass Ejection are likely a major perturbation source either of circumstellar disk evolution and/or of the early planetary system formation (Osten & Wolk 2015; Sanz-Forcada et al. 2011, 2014). The X-IFU will allow us to investigate the initial phase of the intense flares including mass motions as well as their influence on circumstellar disks and/or early planetary evolution.

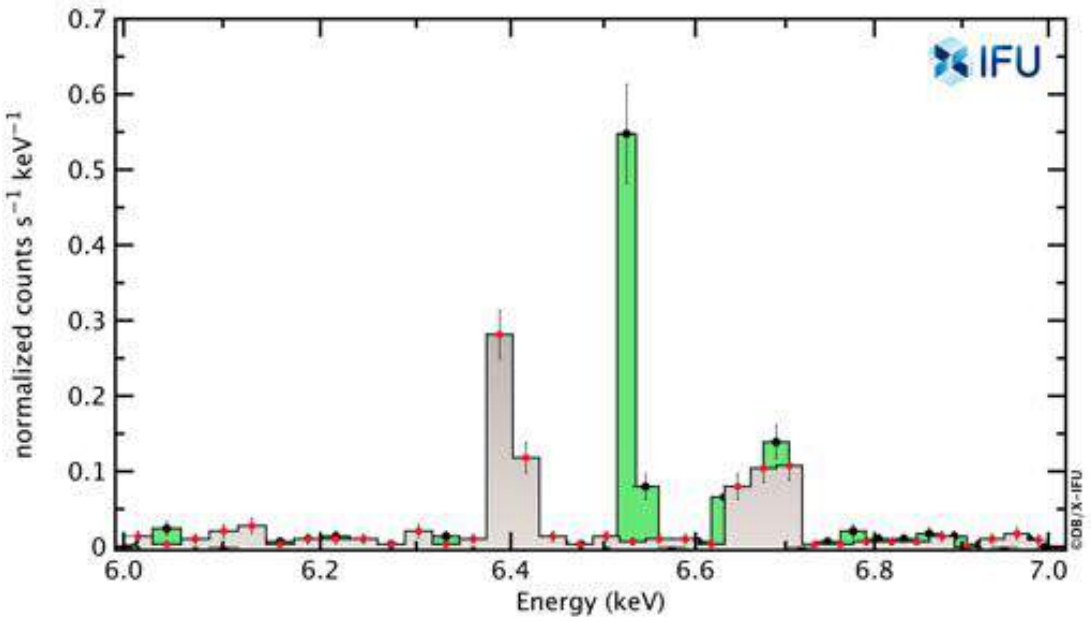

Figure 13 – Simulated X-IFU spectra of Elias 29 in the 6.2-6.8 keV region for a 10 ksec exposure time. Adopted models are derived from the time-resolved spectral analysis of recently obtained XMM-Newton EPIC data that show evidence (at 95% probability level) of time variations of the centroid of the Fe K fluorescent line from the 6.4 keV value expected from neutral material emission up to 6.53 keV. In the two simulated spectra the fluorescent line has been model as a gaussian whose centroids are at 6.4 keV(red) and 6.53 keV (black), respectively while all the other parameters are left unchanged. The best fit model is for the 6.53 keV line. The spectra have been rebinned for plotting purpose to meet the 8σ significance level per bin. The X-IFU will allow to firmly prove the time variation of fluorescent line centroid at the level suggested by EPIC and will allow to determine the ionization status of fluorescent material.

Structures on the surface of late-type stars such as dark star spots or bright plages can be expected to produce corresponding signatures in the outermost atmosphere, the corona, which is traced by X-ray emission. Yet, a clear rotational modulation of the X-ray luminosity has been observed only in few cases (eg., the M star AB Dor, Ref. Hussain et al. (2005)). Joint X-IFU and optical spectropolarimetric monitoring (e.g., with E-ELT/HIRES) will yield unique constraints on the magnetic field structure in active stars, by probing different temperature regimes separately and, consequently, different structures on the stellar surface.

5.4 Supernova Remnants

The X-IFU will provide the spatially-resolved spectral capabilities that have long been wished for in the study of supernova remnants (SNRs) (Decourchelle et al. 2013, and references therein). Like clusters of galaxies, SNRs are extended sources, ranging in angular scale from less than 0.5 arc minutes (in external galaxies) to, in extreme cases, several degrees in our Galaxy. X-IFU will be able to spatially resolve the spectra of SNRs with unprecedented spectral resolution (see Figure 14). This is of great importance to obtain information on the supernova event and explosion mechanism by providing detailed abundance ratios for all elements with Z=6-28 (carbon to nickel) and new insights into the dynamics of the explosion by mapping Doppler shifts/broadening of the ejecta in young SNRs, as well as for understanding the physics of the hot non-equilibrium plasmas in SNRs, its evolution and impact on the interstellar medium.

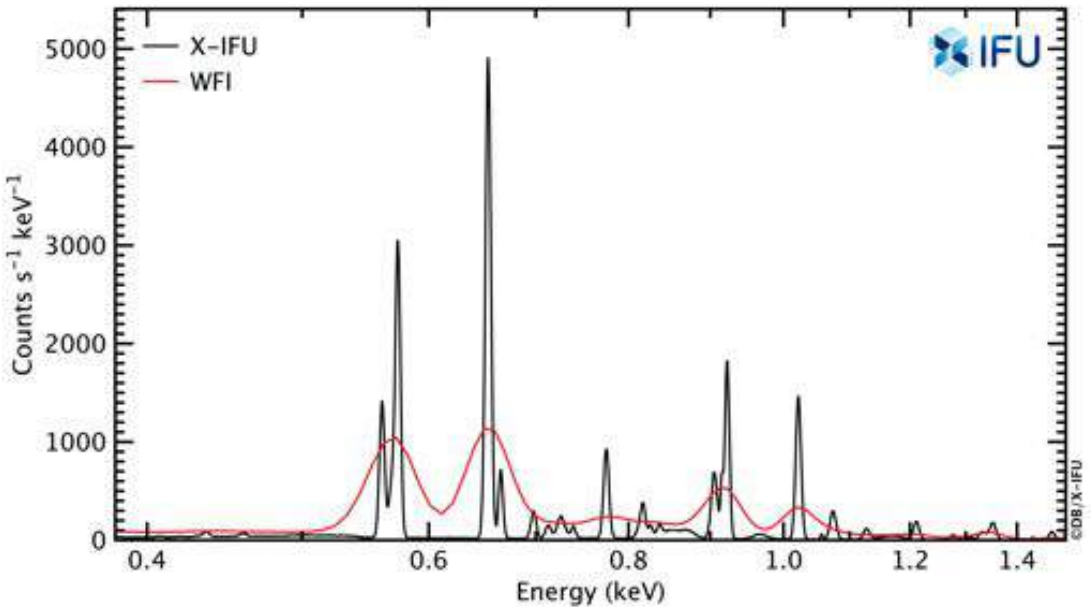

Figure 14 – Illustrating the power of high-resolution X-ray spectroscopy: the SNR 1E 0102.2-7219 is used as a calibration standard in X-ray astronomy. The IACHEC spectral model of the whole remnant (Plucinsky et al. 2017) has been used to simulate the Athena X-IFU and WFI spectra.

To start with the abundance patterns in SNRs, it should be noted that SNRs originate from two different types of explosions: core collapse supernovae (spectroscopy classes Type II, Ib/c) and thermonuclear supernovae (Type Ia). There are still major uncertainties regarding these explosions. Core collapse supernovae

are caused by the implosion of the cores of massive stars, leading to the formation of a neutron star or black hole. How the energy liberated leads to the ejection of the outer envelope is very uncertain, issues being the roles of neutrinos, instabilities, rotation and magnetic field. Thermonuclear supernovae are caused by CO white dwarf which explodes if its masses approaches the Chandrasekhar limit ($1.4\,M_{\odot}$). Here a main issue is the supernova progenitor system, whether the evolution towards this limit is caused by accretion from a normal stellar companion, or due to merging of two white dwarfs. For both types of supernovae much can be learned from the resulting nucleosynthesis products. With the current instruments the more abundant even elements have been reasonably well observed in young SNRs, but it is only with the X-IFU that their 3D distribution can be mapped through line doppler shift and broadening measurements, and their spectral properties along the line of sight determined. This is crucial information for the models of Supernova explosions. Indeed the level of asymmetry of the ejecta is closely related to the explosion mechanism itself, leading to relatively symmetrical explosion for Type Ia compared to core collapse events, and leading to different nucleosynthesis yields.

Different explosion mechanisms leave also distinct patterns in the abundance of the odd elements, like F, Na, Al, P, Sc, Ti, Cr and Mn. These rare elements reveal in core collapse how much the exposure was to intense neutrino radiation, and for thermonuclear supernovae it will inform us about the initial pre-main sequence abundances of the progenitor, but also deviations from nuclear statistical equilibrium reactions, which can be used to distinguish among different types of explosions. X-IFU will be able to detect these weaker lines, among the wealth of lines from more abundant elements and to map their spatial distribution, expected to be in different regions of the SNR, often grouped according to the layer of the supernova in which they were synthesized.

As for the physics of SNRs, the hot plasmas in SNRs are often out of both ionisation equilibrium and thermal equilibrium, as the plasmas often did not have time enough to relax to equilibrium. Ionisation non-equilibrium in young SNRs results in line emission from lower ionisation species than one would expect given the temperature. Low ionisation species can also be enhanced by dust sputtering, releasing new atoms into the hot plasma from broken up dust particles. Interestingly, some older SNRs have plasmas for which the ionisation degree is higher than expected given the electron temperatures. This could arise by rapid adiabatic cooling of the electrons, whereas the recombination rate is too low to keep up with the cooling. With X-IFU, this can be studied in detail, for individual ions, but also as a function of location and will lead to new insights on the progenitor properties (stellar wind, shell) and interstellar environment.

Temperature non-equilibrium means that the electron temperature can be

cooler than the ion temperature. This has important consequences as the electron temperature is easier to measure, but the internal energy is dominated by the ions. With X-IFU the ion temperatures can be measured through the thermal line broadening at the edges of some SNRs, as in the center line broadening will be dominated by different velocities from different parts of the shell. The ion temperatures are also interesting as efficient cosmic-ray acceleration by SNRs shocks may lead to lower ion temperatures (as the internal energy will now be divided between hot plasma and cosmic rays). On the topic of cosmic-ray acceleration, some relatively young SNRs are dominated by X-ray synchrotron radiation. This radiation itself does not need X-IFU to characterise its spectrum, however, X-IFU is important to find signatures of thermal emission, which can be more easily picked up by high resolution spectroscopy. The thermal emission will be used to estimate the plasma densities, which is notably needed to model the gamma-ray emission from these young SNRs.

There are many recent papers discussing the potential of X-IFU to probe supernovae and their progenitors (one white paper entitled *Future X-ray Studies of Supernova Remnants* led by Brian Williams will be submitted as part of the US decadal survey). To take one single example, X-IFU may detect the 5.9-keV Mn K-shell line from the decay of 55 Fe as a promising diagnostic to distinguish between Type Ia supernova (SN Ia) explosion models (Seitenzahl et al. 2015). The 5.9-keV X-ray line provides a distinguishing feature between the observable signatures of two leading explosion scenarios of SNe Ia: a near-Chandrasekhar mass delayed detonation and a violent merger of two white dwarfs. The low rate of SN Ia events in the local Universe and the sensitivities of current generation X-ray observatories make it impossible to constrain the relative rates of SNe Ia from various progenitor models. On the other hand, the X-IFU would enable testing detonation models out to a distance of ~ 5 Mpc. This would make it possible to study future events occurring during its operational life at distances comparable to those of the recent supernovae SN 2011fe (~ 6.4 Mpc) and SN 2014J (~ 3.5 Mpc).

5.5 Neutron Stars and dense matter equation of state

The cores of Neutron Stars (NS) are unique laboratories to probe Quantum Chromodynamics at supranuclear densities and low energies; these conditions cannot be met by accelerators. Yet, models are relatively unconstrained and predict a rich variety of equations of state (EoS) for matter under such extreme conditions, depending on the physics that dominates (e.g., hyperons, Bose-Einstein condensates of pions or kaons, etc.). The only way to probe the EoS of dense matter in

neutron stars is via the measurement of their masses and radii, as each EoS leads to a family of Mass-Radius relations, e.g. Lattimer & Prakash (2001, for a family of representative relations).

X-IFU observations of quiescent Low-Mass X-ray Binaries, especially those residing in globular clusters to minimise uncertainties in the distance, will reveal the apparent neutron star radius. This will be achieved via spectral fitting of the soft X-ray thermal emission of the neutron star surface, folded through appropriate models of their atmosphere. The expectation is that the uncertainty in the measurement of the radius will be of the order of 3% or less, depending on the flux calibration uncertainties. In combination with measurements of the neutron star masses derived from sensitive radial velocity measurements with optical telescopes, Athena measurements will constrain the EoS of dense matter and thence the physics that operates at supranuclear densities.

Zhang et al. (2012) proposed a new technique to determine the mass of compact objects, relying on measuring orbital shifts in the observed energies of absorption lines from disc winds or disc atmospheres as these are expected to trace the motion of the compact object around the centre of mass of the binary system. Following up this proposal, Ponti et al. (2018) have performed spectral simulations of the high inclination system MXB 1659-298, assuming that the ionized plasma is affected by the radial velocity curve of the primary, as observed by Chandra. The X-IFU observations would allow us to determine the amplitude of the radial velocity curve with an uncertainty of $\sim$ 1 %, translating into an uncertainty of $\sim$ 5% on the mass of the neutron star, would the radial velocity of the companion star be known (e.g., via optical spectroscopy).

Additional constraints on the neutron star properties will be inferred from measuring disk reflection by providing insights on the extent of the NS radius, boundary layer, and magnetic field strength, e.g. Ludlam et al. (2017). This will provide further constraints on the equation of state of dense cold matter, with the main advantages being that the distance to the source is not needed and short observations can provide a clear look at Fe Kα emission. This is illustrated in Figure 15, where we show a short 10 kilo-second X-IFU spectrum of the neutron star low-mass X-ray binary 4U1705-44, in which the relativistically broad iron line is clearly seen. The source intensity is about 150 mCrab, and the simulation is performed with the Be filter and a 10 eV resolution.

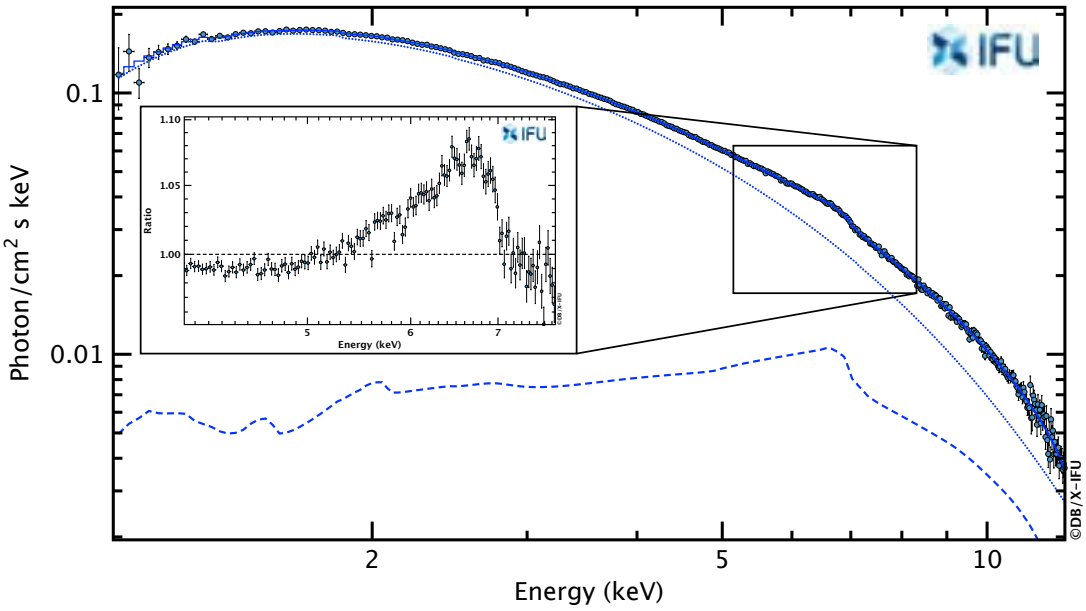

Figure 15 – 10 ks simulated X-IFU spectrum of the neutron star low mass X-ray binary 4U1705-44, assuming the best fit spectral parameters reported by Ludlam et al. (2017) (column 3 of Table 5) from a NuSTAR observation of 28.7 ks duration. The model consists of a disk blackbody (blue dotted line) and a relativistically smeared reflection component assuming an irradiating blackbody continuum from Ballantyne (2004) (blue dashed line). The relativistic blurring kernel assumed is kerrconv (Brenneman & Reynolds 2006). A spin parameter of 0.3 is assumed and solar abundances are set to 1. The inset plot provides a zoom on the relativistically smeared Iron line. The low energy extent of the line provides a constraint on the inner disk radius, hence the neutron star radius which is smaller. In that particular simulation, the inner disk radius is inferred to be twice the radius of the innermost stable circular orbit. The observation is performed with the Be filter. The source intensity is about 150 mCrab.The spectrum has been grouped to a $\sim$ 30 eV per bin (as no narrow spectral features are predicted by the model due to the relativistic smearing).

5.6 Beating the dust

The interstellar medium of our Galaxy (ISM) is a compound of dust and gas formed by atoms, molecules, ions, and electrons. The ISM encodes the history of the star formation and stellar evolution in our Galaxy. Dust is produced in the final stages of stellar evolution, before it gets recycled into new generations of stars and planets. The chemical content of dust is not yet completely understood, although it is established that grains containing O, Mg, Si and Fe are the main constituents of silicates. Silicates, together with carbon, make most of the interstellar dust. Dust can be probed along the line of sight of bright galactic low-mass X-ray binaries, imprinting absorption edges in their otherwise smooth and featureless continuum

spectra (Lee et al. 2009; Costantini et al. 2012; Pinto et al. 2013; Zeegers et al. 2017). The X-ray window is unique as it probes dust in cold ($\leq 10^3$ K) and in hot ($\geq 10^7$ K) over a large range of column densities ($N_H \sim 10^{20} - 10^{24}\,\mathrm{cm}^{-2}$) and contains the K edges of many metals (e.g. carbon, nitrogen, oxygen, neon, and magnesium) as well as the L and K edges of iron, the latter at 7.112 keV enabling the densest regions, e.g. the galactic center, to be probed. The X-IFU will provide breakthrough observations in the chemistry of dust by the combination of unprecedented high count rate capability (enabling bright low-mass X-ray binaries to be observed), spectral resolution and effective area both at 1 and 7 keV.

Iron is of major significance for life. Iron, produced by Supernovae (type Ia or core-collapsed) is heavily depleted in the ISM. It is thought to be included in dusty grains, as a result of cold accretion from the ISM gas onto pre-existing silicate, carbon, or other composite grains (Draine 2009). Using synchrotron data of minerals likely present in the ISM dust, Rogantini et al. (2018) recently studied the capability of X-IFU to probe interstellar dust in the densest regions of the galaxy using iron K-edge. They demonstrated that different chemical compositions of the interstellar dust affecting the shape of the absorption feature beyond the K-edge can be distinguished with single X-IFU observations, along the line of sight of moderately bright low-mass X-ray binaries ($\sim$ 100 mCrab).

5.7 Discovery science through fast ToOs in the era of gravitational waves

Athena will have a fast Target of Opportunity (ToO) observation capability enabling observations of transient phenomena within hours of the trigger. Transients will be very much at the focus of astrophysics by the late 2020s, thanks to facilities like the LSST in the optical, SKA in radio or the all-sky Gamma-ray monitors like SVOM or others. X-IFU observations of some of these triggers will reveal critical astrophysical information on these sources (e.g., on high-z GRBs as explained in Sec. 4.1), extending into the high-energy domain the observations at longer wavelengths.

Likewise, at the end of the next decade, a plethora of gravitational wave sources will be located to an accuracy that will enable follow-up observations with Athena. The kilonova GW170817 has shown (Pian et al. 2017; Smartt et al. 2017) that coalescing compact object in binaries (involving at least a neutron star, with either a stellar mass black hole or another neutron star) will produce, as expected, electromagnetic radiation during the runaway orbital decay due

to gravitational radiation, possibly related also to energetic outflows being generated during the coalescence. A relativistic jet was also found, producing not only a short gamma ray burst Goldstein et al. (2017) but also an X-ray to radio afterglow lasting several days (Troja et al. 2017).

Likewise for high redshift GRBs, X-IFU observations of the X-ray counterparts of compact binary gravitational wave sources would shed light on the nature and properties of their progenitors, their energy output in electromagnetic form, the running of the central engine, as well as on the properties of their host galaxies and circumstellar environments, see e.g. Berger (2014) for a review.

6 From XRISM/Resolve to Athena/X-IFU

The XRISM Resolve spectrometer, a re-flight version of the Hitomi Soft X-ray Spectrometer (Hitomi Collaboration et al. 2016) will be a path finder for Athena X-IFU, and is expected to revolutionize X-ray astronomy. The performance of the two imaging spectrometers in terms of effective area and weak and narrow line sensitivity are compared in Fig. 16.

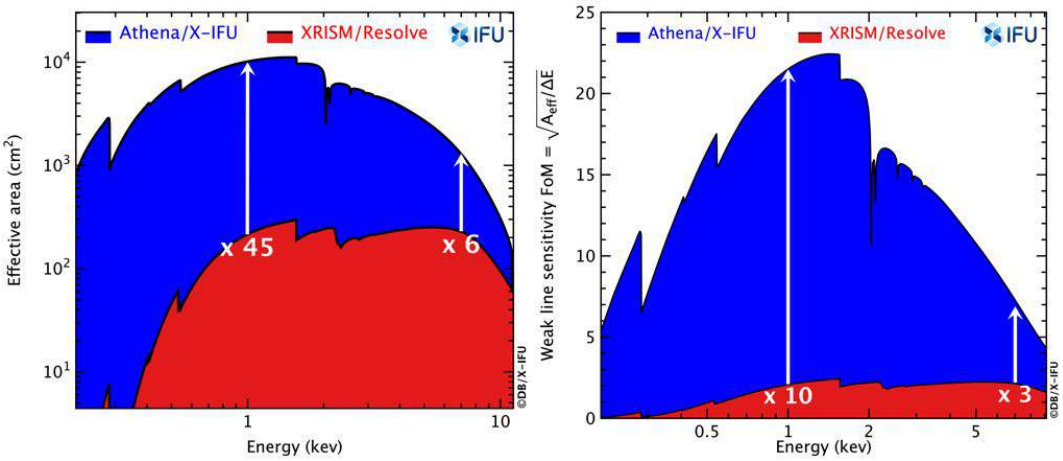

Figure 16 – Left) Effective area comparison between the Athena/X-IFU and XRISM/Resolve instruments. The X-IFU provides an increase of effective area by a factor of 45 and 6 at 1 and 7 keV respectively. Right) Comparison of the weak line sensitivity of the Athena X-IFU and XRISM Resolve spectrometers. The weak line sensitivity scales like the square root of the effective area divided by the spectral resolution. X-IFU provides an order of magnitude increase of sensitivity at 1 keV compared to Resolve.

Beside the leap in sensitivity, the X-IFU will also provide imaging down to 5" scales while the Resolve instrument has pixels of $\sim 1'$ size, and the X-IFU will

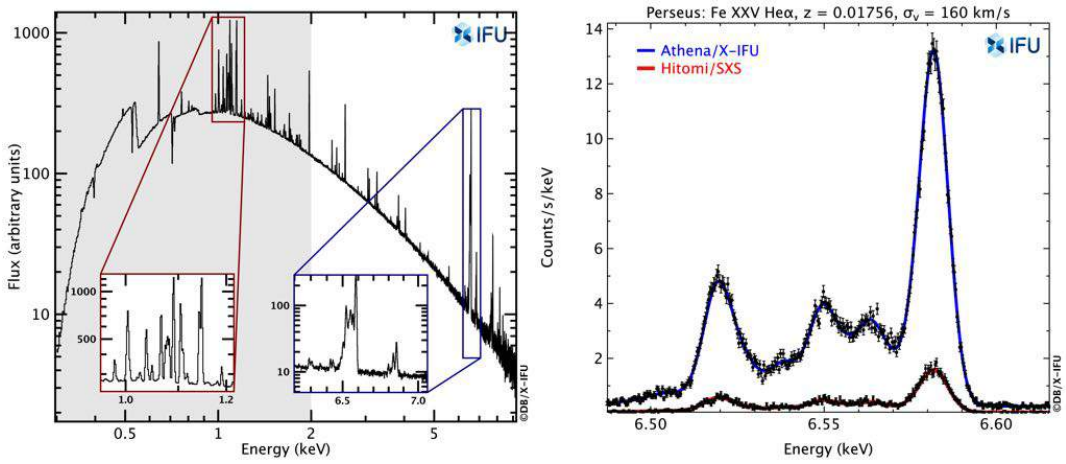

Figure 17 – Left) Broad band simulated Athena X-IFU spectrum of Perseus as derived from the early Hitomi/SXS observation. A zoom on the Iron L and K line complex highlights the wealth of the X-IFU spectrum. The grey area displaying a large number of lines was not observed by Hitomi/SXS. This energy range will be observed by XRISM/Resolve. The data for the plot are courtesy of C. Pinto and A. Fabian. The model is derived from fitting the Hitomi/SXS data. Right) The Athena X-IFU spectrum of the Fe XXV line compared to the one measured with Hitomi Soft X-ray Spectrometer (SXS). This illustrates the improvement in sensitivity due to the effective area increase between the two instruments. The input model is *bapec* with a plasma temperature of 4 keV temperature, metal abundance set to 0.7 and a Gaussian velocity broadening of 160 km/s. The simulation is performed for an integration time of 230 ks, consistent with the length of the early Hitomi observation.

bring the capability to observe bright X-ray sources up to 1 Crab intensities, while the Resolve instrument will only reach $\sim$ 300 mCrab.

The breakthrough capabilities of the X-IFU are further illustrated in Figure 17, which shows the expected X-IFU spectrum of the core of the Perseus cluster, based on the results obtained with the Hitomi Soft X-ray Spectrometer (Hitomi Collaboration et al. 2016).

7 Acknowledgements

This paper has been prepared with the support of the X-IFU Science Advisory Team, but benefited from the inputs from many members of the X-IFU Consortium, who should be acknowledged here. DB is grateful to E. Costantini, C. Pinto and D. Lin for providing inputs.

References

Altamirano, D., Belloni, T., Linares, M., et al. 2011, ApJL, 742, L17

Anders, E. & Grevesse, N. 1989, Geochimica et Cosmochimica Acta, 53, 197

Argiroffi, C., Flaccomio, E., Bouvier, J., et al. 2011, Astronomy and Astrophysics, 530, A1

Armitage, P. J. & Reynolds, C. S. 2003, Monthly Notices of the Royal Astronomical Society, 341, 1041

Balbus, S. A. & Hawley, J. F. 1991, The Astrophysical Journal, 376, 214

Ballantyne, D. R. 2004, Monthly Notices of the Royal Astronomical Society, 351, 57

Barret, D., Lam Trong, T., den Herder, J.-W., et al. 2016, in Proceedings of the International Society for Optical Engineering, Vol. 9905, Space Telescopes and Instrumentation 2016: Ultraviolet to Gamma Ray, 99052F

Begelman, M. C., Armitage, P. J., & Reynolds, C. S. 2015, The Astrophysical Journal, 809, 118

Belloni, T., Klein-Wolt, M., Méndez, M., van der Klis, M., & van Paradijs, J. 2000, Astronomy and Astrophysics, 355, 271

Belloni, T., Méndez, M., King, A. R., van der Klis, M., & van Paradijs, J. 1997, ApJL, 488, L109

Berger, E. 2014, Annual Review of Astronomy and Astrophysics, 52, 43

Berti, E. & Volonteri, M. 2008, The Astrophysical Journal, 684, 822

Bertschinger, E. 1998, ARAA, 36, 599

Biffi, V., Planelles, S., Borgani, S., et al. 2018, Monthly Notices of the Royal Astronomical Society, 476, 2689

Blandford, R. D. & Payne, D. G. 1982, Monthly Notices of the Royal Astronomical Society, 199, 883

Boehringer, H., Voges, W., Fabian, A. C., Edge, A. C., & Neumann, D. M. 1993, Monthly Notices of the Royal Astronomical Society, 264, L25

Boyle, B. J., Shanks, T., & Peterson, B. A. 1988, Monthly Notices of the Royal Astronomical Society, 235, 935

Brandt, W. N. & Hasinger, G. 2005, ARAA, 43, 827

Brenneman, L. 2013, Acta Polytechnica, 53, 652

Brenneman, L. W. & Reynolds, C. S. 2006, The Astrophysical Journal, 652, 1028

Brickhouse, N. S., Cranmer, S. R., Dupree, A. K., Luna, G. J. M., & Wolk, S. 2010, The Astrophysical Journal, 710, 1835

Cappi, M., Done, C., Behar, E., et al. 2013, arXiv e-prints, 1306.2330

Cazorla, C. & Nazé, Y. 2017, Astronomy and Astrophysics, 608, A54

Chartas, G., Brandt, W. N., & Gallagher, S. C. 2003, The Astrophysical Journal, 595, 85

Chartas, G., Brandt, W. N., Gallagher, S. C., & Garmire, G. P. 2002, The Astrophysical Journal, 579, 169

Chartas, G., Eracleous, M., Dai, X., Agol, E., & Gallagher, S. 2007, The Astrophysical Journal, 661, 678

Chatterjee, R., Marscher, A. P., Jorstad, S. G., et al. 2011, The Astrophysical Journal, 734, 43

Chatterjee, R., Marscher, A. P., Jorstad, S. G., et al. 2009, The Astrophysical Journal, 704, 1689

Churazov, E., Vikhlinin, A., Zhuravleva, I., et al. 2012, Monthly Notices of the Royal Astronomical Society, 421, 1123

Clavel, M., Terrier, R., Goldwurm, A., et al. 2013, Astronomy and Astrophysics, 558, A32

Costantini, E., Pinto, C., Kaastra, J. S., et al. 2012, Astronomy and Astrophysics, 539, A32

Cucchetti, E., Pointecouteau, E., Peille, P., et al. 2018, Astronomy and Astrophysics, 620, A173

Dadina, M., Vignali, C., Cappi, M., et al. 2018, Astronomy and Astrophysics, 610, L13

de La Calle Pérez, I., Longinotti, A. L., Guainazzi, M., et al. 2010, Astronomy and Astrophysics, 524, A50

de Marco, B., Iwasawa, K., Cappi, M., et al. 2009, Astronomy and Astrophysics, 507, 159

Decourchelle, A., Costantini, E., Badenes, C., et al. 2013, ArXiv e-prints, 1306.2335

Dovčiak, M., Bianchi, S., Guainazzi, M., Karas, V., & Matt, G. 2004, Monthly Notices of the Royal Astronomical Society, 350, 745

Draine, B. T. 2009, in Astronomical Society of the Pacific Conference Series, Vol. 414, Cosmic Dust - Near and Far, ed. T. Henning, E. Grün, & J. Steinacker, 453

Dunn, R. J. H., Fender, R. P., Körding, E. G., Belloni, T., & Cabanac, C. 2010, Monthly Notices of the Royal Astronomical Society, 403, 61

Fabian, A. C., Iwasawa, K., Reynolds, C. S., & Young, A. J. 2000, PASP, 112, 1145

Fragile, P. C. & Blaes, O. M. 2008, The Astrophysical Journal, 687, 757

Fukumura, K., Kazanas, D., Contopoulos, I., & Behar, E. 2010, The Astrophysical Journal, 715, 636

Gal-Yam, A., Maoz, D., Guhathakurta, P., & Filippenko, A. V. 2003, AJ, 125, 1087

Georgakakis, A., Carrera, F., Lanzuisi, G., et al. 2013, ArXiv e-prints

Giardino, G., Favata, F., Pillitteri, I., et al. 2007, Astronomy and Astrophysics, 475, 891

Glassgold, A. E., Feigelson, E. D., & Montmerle, T. 2000, Protostars and Planets IV, 429

Goldstein, A., Veres, P., Burns, E., et al. 2017, The Astrophysical Journal Letters, 848, L14

Heger, A. & Woosley, S. E. 2010, The Astrophysical Journal, 724, 341

Hitomi Collaboration, Aharonian, F., Akamatsu, H., et al. 2016, Nature, 535, 117

Hussain, G. A. J., Brickhouse, N. S., Dupree, A. K., et al. 2005, The Astrophysical Journal, 621, 999

Iwasawa, K., Miniutti, G., & Fabian, A. C. 2004, Monthly Notices of the Royal Astronomical Society, 355, 1073

Janiuk, A., Grzedzielski, M., Capitanio, F., & Bianchi, S. 2015, Astronomy and Astrophysics, 574, A92

Janiuk, A. & Misra, R. 2012, Astronomy and Astrophysics, 540, A114

Jonker, P., O'Brien, P., Amati, L., et al. 2013a, ArXiv e-prints, 1306.2336

Jonker, P., O'Brien, P., Amati, L., et al. 2013b, arXiv e-prints, 1306.2336

Kammoun, E. S., Risaliti, G., Stern, D., et al. 2017, Monthly Notices of the Royal Astronomical Society, 465, 1665

Khatri, R. & Gaspari, M. 2016, ArXiv e-prints, 1604.03106

King, A. & Pounds, K. 2015, ARAA, 53, 115

King, A. R. 2010, Monthly Notices of the Royal Astronomical Society, 402, 1516

Kirkpatrick, C. C., McNamara, B. R., & Cavagnolo, K. W. 2011, The Astrophysical Journal, 731, L23

Kormendy, J. & Richstone, D. 1995, ARAA, 33, 581

Lanzuisi, G., Giustini, M., Cappi, M., et al. 2012, Astronomy and Astrophysics, 544, A2

Lattimer, J. M. & Prakash, M. 2001, The Astrophysical Journal, 550, 426

Lau, E. T., Nagai, D., & Nelson, K. 2013, The Astrophysical Journal, 777, 151

Lee, J. C., Xiang, J., Ravel, B., Kortright, J., & Flanagan, K. 2009, The Astrophysical Journal, 702, 970

Lightman, A. P. & Eardley, D. M. 1974, ApJL, 187, L1

Lin, D., Maksym, P. W., Irwin, J. A., et al. 2015, The Astrophysical Journal, 811, 43

Lin, D., Strader, J., Carrasco, E. R., et al. 2018, Nature Astronomy, 2, 656

Livio, M., Pringle, J. E., & King, A. R. 2003, The Astrophysical Journal, 593, 184

Ludlam, R. M., Miller, J. M., Bachetti, M., et al. 2017, The Astrophysical Journal, 836, 140

Madau, P., Ferguson, H. C., Dickinson, M. E., et al. 1996, Monthly Notices of the Royal Astronomical Society, 283, 1388

Magorrian, J., Tremaine, S., Richstone, D., et al. 1998, AJ, 115, 2285

Markevitch, M. & Vikhlinin, A. 2007, Phys Rep, 443, 1

Martocchia, S., Piconcelli, E., Zappacosta, L., et al. 2017, Astronomy and Astrophysics, 608, A51

McCarthy, I. G., Bower, R. G., Balogh, M. L., et al. 2007, Monthly Notices of the Royal Astronomical Society, 376, 497

McNamara, B. R., Nulsen, P. E. J., Wise, M. W., et al. 2005, Nature, 433, 45

Miller, J. M., Raymond, J., Fabian, A. C., et al. 2016, ApJL, 821, L9

Mitchell, R. J., Culhane, J. L., Davison, P. J. N., & Ives, J. C. 1976, Monthly Notices of the Royal Astronomical Society, 175, 29P

Mitsuda, K., Kelley, R. L., Akamatsu, H., et al. 2014, in Proc. SPIE, Vol. 9144, Space Telescopes and Instrumentation 2014: Ultraviolet to Gamma Ray, 91442A

Molendi, S., Eckert, D., De Grandi, S., et al. 2016, Astronomy and Astrophysics, 586, A32

Nagai, D., Lau, E. T., Avestruz, C., Nelson, K., & Rudd, D. H. 2013, The Astrophysical Journal, 777, 137

Nandra, K., Barret, D., Barcons, X., et al. 2013, ArXiv e-prints, 1306.2307

Nandra, K., O'Neill, P. M., George, I. M., & Reeves, J. N. 2007, Monthly Notices of the Royal Astronomical Society, 382, 194

Nazé, Y., Ramiaramanantsoa, T., Stevens, I. R., Howarth, I. D., & Moffat, A. F. J. 2018, Astronomy and Astrophysics, 609, A81

Nicastro, F., Kaastra, J., Krongold, Y., et al. 2018, Nature, 558, 406

Oskinova, L. M., Nazé, Y., Todt, H., et al. 2014, Nature Communications, 5, 4024

Osten, R. A. & Wolk, S. J. 2015, The Astrophysical Journal, 809, 79

Pian, E., D'Avanzo, P., Benetti, S., et al. 2017, Nature, 551, 67

Pillitteri, I., Flaccomio, E., Reale, F., & et, a. 2018, Astronomy and astrophysics, submitted

Pinto, C., Kaastra, J. S., Costantini, E., & de Vries, C. 2013, Astronomy and Astrophysics, 551, A25

Pinto, C., Middleton, M. J., & Fabian, A. C. 2016, Nature, 533, 64

Pinto, C., Sanders, J. S., Werner, N., et al. 2015, Astronomy and Astrophysics, 575, A38

Planelles, S., Schleicher, D. R. G., & Bykov, A. M. 2015, Space Science Reviews, 188, 93

Plucinsky, P. P., Beardmore, A. P., Foster, A., et al. 2017, Astronomy and Astrophysics, 597, A35

Ponti, G., Bianchi, S., Muñoz-Darias, T., & Nandra, K. 2018, Monthly Notices of the Royal Astronomical Society, 481, L94

Ponti, G., Morris, M. R., Terrier, R., & Goldwurm, A. 2013, in Astrophysics and Space Science Proceedings, Vol. 34, Cosmic Rays in Star-Forming Environments, ed. D. F. Torres & O. Reimer, 331

Pounds, K. A., Reeves, J. N., King, A. R., et al. 2003, Monthly Notices of the Royal Astronomical Society, 345, 705

Proga, D. & Kallman, T. R. 2004, The Astrophysical Journal, 616, 688

Rasia, E., Borgani, S., Murante, G., et al. 2015, The Astrophysical Journal Letters, 813, L17

Rauw, G., Mossoux, E., & Nazé, Y. 2016, New Astronomy, 43, 70

Reeves, J. N., Braito, V., Nardini, E., et al. 2018, The Astrophysical Journal Letters, 854, L8

Remillard, R. A. & McClintock, J. E. 2006, ARAA, 44, 49

Reynolds, C. S. 2014, Space. Sci. Rev., 183, 277

Reynolds, M. T. & Miller, J. M. 2013, The Astrophysical Journal, 769, 16

Risaliti, G., Harrison, F. A., Madsen, K. K., et al. 2013, Nature, 494, 449

Rogantini, D., Costantini, E., Zeegers, S. T., et al. 2018, Astronomy and Astrophysics, 609, A22

Roncarelli, M., Gaspari, M., Ettori, S., et al. 2018, Astronomy & Astrophysics, 618, A39

Sanders, J. S. & Fabian, A. C. 2013, Monthly Notices of the Royal Astronomical Society, 429, 2727

Sanz-Forcada, J., Desidera, S., & Micela, G. 2014, Astronomy and Astrophysics, 570, A50

Sanz-Forcada, J., Micela, G., Ribas, I., et al. 2011, Astronomy and Astrophysics, 532, A6

Schekochihin, A. A. & Cowley, S. C. 2007, Turbulence and Magnetic Fields in Astrophysical Plasmas, ed. S. Molokov, R. Moreau, & H. K. Moffatt (Springer), 85

Schindler, S. & Diaferio, A. 2008, Space Sci Rev, 134, 363

Sciortino, S., Flaccomio, E., Pillitteri, I., & Reale, F. 2018, Astronomy Now, in press

Sciortino, S., Rauw, G., Audard, M., et al. 2013, arXiv e-prints, 1306.2333

Seitenzahl, I. R., Summa, A., Krauß, F., et al. 2015, Monthly Notices of the Royal Astronomical Society, 447, 1484

Shakura, N. I. & Sunyaev, R. A. 1973, Astronomy and Astrophysics, 24, 337

Sim, S. A., Miller, L., Long, K. S., Turner, T. J., & Reeves, J. N. 2010, Monthly Notices of the Royal Astronomical Society, 404, 1369

Smartt, S. J., Chen, T.-W., Jerkstrand, A., et al. 2017, Nature, 551, 75

Strickland, D. K. & Stevens, I. R. 2000, Monthly Notices of the Royal Astronomical Society, 314, 511

Takahashi, T., Mitsuda, K., Kelley, R., et al. 2014, in Proc. SPIE, Vol. 9144, Space Telescopes and Instrumentation 2014: Ultraviolet to Gamma Ray, 914425

Tombesi, F., Cappi, M., Reeves, J. N., et al. 2010a, Astronomy and Astrophysics, 521, A57

Tombesi, F., Meléndez, M., Veilleux, S., et al. 2015, Nature, 519, 436

Tombesi, F., Sambruna, R. M., Reeves, J. N., et al. 2010b, The Astrophysical Journal, 719, 700

Troja, E., Piro, L., van Eerten, H., et al. 2017, Nature, 551, 71

ud-Doula, A. & Nazé, Y. 2016, Advances in Space Research, 58, 680

Vignali, C., Iwasawa, K., Comastri, A., et al. 2015, Astronomy and Astrophysics, 583, A141

Vogelsberger, M., Genel, S., Springel, V., et al. 2014, Monthly Notices of the Royal Astronomical Society, 444, 1518

Walton, D. J., Nardini, E., Fabian, A. C., Gallo, L. C., & Reis, R. C. 2013, Monthly Notices of the Royal Astronomical Society, 428, 2901

Wang, Q. D., Nowak, M. A., Markoff, S. B., et al. 2013, Science, 341, 981

Wilms, J., Brand, T., Barret, D., et al. 2014, in Proceedings of the International Society for Optical Engineering, Vol. 9144, Space Telescopes and Instrumentation 2014: Ultraviolet to Gamma Ray, 91445X

Yaqoob, T. & Padmanabhan, U. 2004, The Astrophysical Journal, 604, 63

Zeegers, S. T., Costantini, E., de Vries, C. P., et al. 2017, Astronomy and Astrophysics, 599, A117

Zhang, S.-N., Liao, J., & Yao, Y. 2012, Monthly Notices of the Royal Astronomical Society, 421, 3550

Zhuravleva, I., Churazov, E., Schekochihin, A. A., et al. 2014, Nature, 515, 85